Hydro-biogeochemical impacts of fugitive methane on a shallow unconfined aquifer

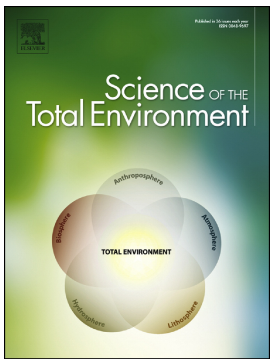

Hydro-biogeochemical impacts of fugitive methane on a shallow unconfined aquifer

Olenka N. Forde, Aaron G. Cahill, K. Ulrich Mayer, Bernhard Mayer, Rachel L. Simister, Niko Finke, Sean A. Crowe, John A. Cherry, Beth L. Parker

PII: S0048-9697(19)32895-5
DOI: https://doi.org/10.1016/j.scitotenv.2019.06.322
Reference: STOTEN 32976

To appear in: *Science of the Total Environment*

Received date: 12 April 2019
Revised date: 20 June 2019
Accepted date: 20 June 2019

Please cite this article as: O.N. Forde, A.G. Cahill, K.U. Mayer, et al., Hydro-biogeochemical impacts of fugitive methane on a shallow unconfined aquifer, Science of the Total Environment, https://doi.org/10.1016/j.scitotenv.2019.06.322

Hydro-Biogeochemical Impacts of Fugitive Methane on a Shallow Unconfined Aquifer

Olenka N. Forde[1], Aaron G. Cahill[2,1,3], K. Ulrich Mayer[1], Bernhard Mayer[4], Rachel L. Simister[1,5], Niko Finke[1,5], Sean A. Crowe[1,5], John A. Cherry[2], Beth L. Parker[2]

1. Department of Earth, Ocean and Atmospheric Sciences, University of British Columbia, 2020-2007 Main Mall, Vancouver, BC, V6T 1Z4, Canada

2. G360 Institute for Groundwater Research, College of Engineering and Physical Sciences, University of Guelph, 50 Stone Road East, Guelph, ON, N1G 2W1, Canada

3. Heriot-Watt University, Lyell Centre, Research Avenue South, Edinburgh, EH14 4AP, United Kingdom

4. Department of Geoscience, University of Calgary, 2500 University Drive NW, Calgary, AB, T2N 1N4, Canada

5. Department of Microbiology and Immunology, University of British Columbia, 2350 Health Sciences Mall, Vancouver, BC, V6T 1Z3, Canada

*Corresponding author (oforde@eoas.ubc.ca)

Highlights

1. Two biogeochemical stages evolved during and post natural gas injection
2. Gas injection led to upward displacement of groundwater with elevated TDS
3. Dissolved methane persisted in groundwater >700 days post natural gas release

4. Aerobic and anaerobic methane oxidation was limited and spatially discrete
5. pH and geochemical changes were limited by carbonate mineral dissolution

Abstract

Oil and gas development can result in natural gas migration into shallow groundwater. Methane (CH_4), the primary component of natural gas, can subsequently react with solutes and minerals in the aquifer to create byproducts that affect groundwater chemistry. Hydro-biogeochemical processes induced by fugitive gas from leaky oil and gas wells are currently not well understood. We monitored the hydro-biogeochemical responses of a controlled natural gas release into a well-studied Pleistocene beach sand aquifer (Canadian Forces Base Borden, Ontario, Canada). Groundwater samples were collected before, during, and up to 700 days after gas injection and analyzed for pH, major and minor ions, alkalinity, dissolved gases, stable carbon isotope ratios of CO_2 and CH_4, and microbial community composition. Gas injection resulted in a dispersed plume of free and dissolved phase natural gas, affecting groundwater chemistry in two distinct temporal phases. Initially (i.e. during and immediately after gas injection), pH declined and major ions and trace elements fluctuated; at times increasing above baseline concentrations. Changes in the short-term were due to invasion of deep groundwater with elevated total dissolved solids entrained with the upward migration of free phase gas and, reactions that were instigated through the introduction of constituents other than CH_4 present in the injected gas (e.g. CO_2). At later times, more pronounced aerobic and anaerobic CH_4 oxidation led to subtle increases in major ions (e.g. Ca^{2+}, H_4SiO_4) and trace elements (e.g. As, Cr). Microbial community profiling indicated a persistent perturbation to community composition with a conspicuous ingrowth of taxa implicated in aerobic CH_4 oxidation as well anaerobic S, N and Fe species metabolism.

Keywords

aqueous geochemistry; gas migration; groundwater; hydro-biogeochemistry; methane; natural gas; methane oxidation.

Abbreviations

bgs, below ground surface; CFB, Canadian Forces Base; DOC, dissolved organic carbon; EC, electrical conductivity; GM, gas migration; ID, inside diameter; M1-31, multilevel well 1-31; MCL, maximum contaminant level; PE, polyethylene; TDS, total dissolved solids; TIC, total inorganic carbon.

1. Introduction

Recent increases in shale gas development, conducted by horizontal drilling and hydraulic fracturing, have drawn attention to the issue of subsurface gas leakage from compromised oil and gas wells (CCA, 2014; Dusseault and Jackson, 2014; Vidic et al., 2013). Natural gas can escape from a wellbore casing and result in fugitive gas migration (GM) in the surrounding geologic material (Cahill et al., 2019). Gas migration can also arise during drilling if pathways are formed along the well bore, mobilizing non-target reservoir gas at an intermediate depth (i.e. non-economic gas-rich strata between a target petroleum reservoir and shallow groundwater resources) (Dusseault and Jackson, 2014). Although well leakage has been historically documented and investigated (Dyck and Dunn, 1986; Gurevich et al., 1993; Harrison, 1983;

Kelly et al., 1985), the debate on the occurrence and impacts of GM has been re-ignited with the advent of shale gas development. In addition to creating a potential explosion hazard (Kelly et al., 1985; Williams and Aitkenhead, 1991), a primary concern related to GM is for natural gas constituents (i.e. methane (CH_4), ethane (C_2H_6) and propane (C_3H_8)) to ingress into aquifers containing potable groundwater and induce hydro-geochemical changes (Vengosh et al., 2014; Vidic et al., 2013). For the most part, recent research on fugitive gas and groundwater has taken an environmental forensics approach aiming to identify the origins of CH_4 in groundwater around regions of oil and gas development (Darrah et al., 2014; Humez et al., 2016a; Li and Carlson, 2014; Molofsky et al., 2016). However, few studies have specifically focused on the direct or indirect impacts of fugitive gas on aqueous geochemistry and the mechanisms by which they occur.

While dissolved CH_4 ($CH_{4(aq)}$) itself is non-toxic in drinking water, it can be utilized as a carbon source in microbial metabolic pathways causing the release of major ions and trace elements that can negatively affect water chemistry (Gorody, 2012). Such microbially mediated reactions occur based on availability of electron acceptors and their thermodynamic favourability (i.e. in order of the redox sequence, Table S1) (Christensen et al., 2000). These redox reactions also apply to C_2H_6 and C_3H_8 (Table S1). If dissolved oxygen ($O_{2(aq)}$) is present in groundwater, aerobic oxidation of $CH_{4(aq)}$ will proceed first and produce dissolved carbon dioxide ($CO_{2(aq)}$) and water. Carbonic acidification, from $CO_{2(aq)}$ generation, is well known to affect groundwater chemistry by inducing dissolution of acid soluble/reactive minerals and the release of undesirable trace elements (Cahill et al., 2014; Cahill and Jakobsen, 2013). Once $O_{2(aq)}$ is depleted, or in the case of anoxic groundwater systems where none is present, $CH_{4(aq)}$ oxidation can be coupled to less energetically favorable electron acceptors. Anaerobic $CH_{4(aq)}$ oxidation involves reduction of

other dissolved species and/or reductive dissolution of solid phases present in the aquifer matrix (i.e. NO_3^-, Mn/Fe oxides and/or SO_4^{2-}, Table S1). These processes typically lead to an increase in alkalinity and other aqueous species byproducts (e.g. $N_{2(aq)}$, $H_2S_{(aq)}/HS^-$, Fe^{2+}, Mn^{2+} and any associated trace elements), with impacts on water chemistry. In the field, anaerobic oxidation of fugitive $CH_{4(aq)}$ has been observed and attributed to reduction of Fe- and Mn-oxides (Schout et al., 2017) and SO_4^{2-} (Van Stempvoort et al., 2005; Wolfe et al., 2017). Anaerobic $CH_{4(aq)}$ oxidation has also been observed in landfill leachate plumes (Christensen et al., 2000; Grossman et al., 2002) and aquifers contaminated with petroleum hydrocarbons (e.g.: Amos et al., 2012). Although $CH_{4(aq)}$ oxidation is generally well understood, more research is needed in the context of natural gas leakage to characterize the interacting processes that lead to fugitive CH_4 attenuation and/or secondary groundwater impacts.

Upward migration of deep saline fluids and entrainment with shallow potable groundwater could also contribute to deleterious changes in water chemistry around natural gas wells. Deep formation fluid migration to shallower groundwater has been observed in unconsolidated aquifers in the presence of faults (Bordeleau et al., 2018; Gumm et al., 2016). Studies have also measured elevated brine constituents (e.g. Na^+, Cl^-, Br^-) in groundwater wells around regions of shale gas development (Kreuzer et al., 2018; McPhillips et al., 2014; Warner et al., 2012; Yan et al., 2017). While various factors can contribute to saline groundwater in shallower aquifers, one possible explanation is the presence of pathways for deeper formation water to migrate vertically and become entrained with shallower water. However, it is currently difficult to attribute a direct link to oil and gas development and the mechanisms associated with such processes are not well characterized.

While concerns regarding fugitive CH_4 in groundwater persist, there remains limited knowledge of the hydro-biogeochemical processes that occur in aquifers during and after natural gas leakage. A controlled natural gas release experiment was recently conducted in a shallow unconfined aquifer at the Canadian Forces Base (CFB) Borden, Ontario, Canada. The experiment provided an opportunity to monitor the migration, impacts, and fate of simulated natural gas leakage in groundwater through a comprehensive multi-disciplinary approach (Cahill et al., 2017). Overall, it was shown that free phase gas was highly mobile in the unconsolidated, unconfined shallow aquifer. A relatively small volume release over a short timescale (i.e. 51 m^3 at standard temperature and pressure in 72 days) generated an extensive and dispersed plume of free and dissolved phase natural gas (Cahill et al., 2018, 2017; Forde et al., 2018; Steelman et al., 2017). Migration of the free phase gas, and consequently the volume of the impacted aquifer, were controlled by buoyancy and small-scale heterogeneities in sedimentary architecture. Vadose zone and surface efflux measurements up to day 87 indicate that at least half of the injected gas remained in the subsurface (Forde et al., 2018).

Here, we present high-resolution spatial aqueous chemistry data (including major ions, trace elements, alkalinity, dissolved gases and stable carbon isotope ratios of $CO_{2(aq)}$ and $CH_{4(aq)}$) for samples collected before, during, and up to 700 days after the simulated natural gas release, and microbial community profiles from day 0-700. This paper follows a comprehensive review on the fate of dissolved gases during and shortly after injection (day 0 to 300) (Cahill et al., 2018) and reveals long-term trends (day 300 to 700) with secondary groundwater impacts. The objectives of this study were to: i) assess the long-term evolution of dissolved gases as a result of fugitive gas migration into a shallow unconfined aquifer; ii) characterize the occurrence and extent of fugitive CH_4 oxidation; iii) evaluate changes in aqueous geochemistry as a consequence

of fugitive gas migration and $CH_{4(aq)}$ oxidation; and iv) discuss biogeochemical processes occurring in the short- and longer-term resulting from migration of fugitive gas into a shallow unconfined aquifer.

2. Materials and Methods

2.1 Field Site Geologic Setting

The natural gas release was conducted within CFB Borden, Ontario, Canada (Figure 1a). The aquifer at this site has been well characterized through previous studies on solid phase composition (Ball et al., 1990), groundwater flow (MacFarlane et al., 1983), hydrogeochemistry (Nicholson et al., 1983), and physical heterogeneity (Sudicky, 1986). The aquifer therefore provided a tractable setting to study the fate of natural gas through a controlled release experiment and associated hydrogeochemical impacts. In the experimental area within CFB Borden, the unconfined aquifer is composed of clean, well-sorted medium- to fine-grained silty sand with silt, silty clay, and coarse sand lenses underlain by a clayey silt aquitard and with a water table at ~1 m (fluctuating ± 0.5 m seasonally) below ground surface (bgs) (Sudicky and Illman, 2011). As part of the current study, a detailed interrogation of the sedimentary architecture was performed through depth-discrete grain size analyses on multiple cores, the results of which are described in detail by Steelman et al. (2017) and Cahill et al. (2018). Historically, the aquifer material is documented to be dominated by calcareous sand with few clay minerals and low organic carbon content (0.02 to 0.09 %) (Ball et al., 1990; Mackay et al., 1986). Quartz is the predominant mineral followed by feldspar, carbonates, and to a lesser extent amphibole and chlorite (Mackay et al., 1986).

Studies from the 1980s categorized the aquifer into an upper uncontaminated region (from water table to ~7 m bgs), and a lower contaminated region (~8 m to 9 m bgs) due to the presence of a landfill-derived contaminant plume (Butler et al., 1997; MacFarlane et al., 1983). Groundwater in the uncontaminated aquifer was characterized by low levels of $O_{2(aq)}$ (<0.003 mmol L^{-1}, decreasing with depth), a narrow range in pH (6.8 to 8.0), total dissolved solids (TDS) ranging from 380 to 500 mg L^{-1}, electrical conductivity (EC, ~500 µS cm^{-1}), Cl^- between 0.03 to 0.08 mmol L^{-1}, and SO_4^{2-} ranging from 0.1 to 0.3 mmol L^{-1} (Mackay et al., 1986; MacFarlane et al., 1983; Nicholson et al., 1983). Landfill contaminated groundwater was defined by elevated SO_4^{2-} (9.6 mmol L^{-1}), Cl^- (4.3 mmol L^{-1}), TDS (2300 mg L^{-1}), and EC (1500 µS cm^{-1}) (MacFarlane et al., 1983; Nicholson et al., 1983). The contaminant plume exhibited anoxic conditions as indicated by the presence of Fe^{2+} (0.5 mmol L^{-1}) and $O_{2(aq)}$ below detection (1 µmol L^{-1}). The pH in the landfill leachate plume was similar to that of the uncontaminated water, ranging from 6.8 to 7.9 pH units (Nicholson et al., 1983). Present day, hydrogeologic conditions remain similar and the landfill leachate is still noticeable at the base of the aquifer (~7 m bgs and below). Notably, groundwater with elevated TDS is also common in regions of oil and gas development (Botner et al., 2018; Hildenbrand et al., 2015; Humez et al., 2016b). Therefore, the groundwater conditions found in the lower part of the Borden aquifer mimic those in aquifers that may be affected by fugitive GM.

2.2 Injection Infrastructure and Regime

Simulated natural gas (93.8 % CH_4, 3.8 % C_2H_6, 0.3 % C_3H_8, ~0.1 % C_{4+}, 1.1 % N_2, 0.8 % CO_2) was delivered to the subsurface through two 45^o inclined sparging wells at depths of 4.5 m and 9 m bgs. The injected gas also contained a small amount of O_2 (0.05 %) introduced during

manufacturing of the gas mixture. Inclined sparging wells were used to minimize vertical GM along the injection tubing. The sparging wells were comprised of 1-m long porous polyethylene (PE) well screens [SCHUMASOIL®]) connected to gas cylinders with 0.006 m (inside diameter [ID]) PE tubing, via a mass flow control-valve (Red-y smart GSC-C9SA-BB26) that was regulated by associated software (Get Red-y, Vögtlin Instruments AG, Switzerland). Over 72 days a total of 51 m^3 (at standard temperature and pressure) of simulated natural gas was injected at progressively increasing rates starting with the lowest rate of 0.2 m^3 day^{-1} and ending with the highest rate of 4.3 m^3 day^{-1} (Table S2). The injection rates were maintained continuously, except from day 38 to 42, when injection was interrupted due to a power outage on site. Injection wells were closed with non-return valves post injection.

2.3 Monitoring Network

Multilevel sampling wells were installed around the sparge wells and across the site using a Geoprobe (model 7822DT) direct push system. Each well was comprised of 0.006 m ID PE tubing with a 5-cm geotextile screen (Nitex monofilament screen cloth, 200 μm mesh) fixed to a polyvinyl-chloride center-stock. In total, 32 multilevel wells (M1 – M32, 122 sampling points) were screened at different intervals with either: three screens (2 m, 5 m and 8 m bgs); four screens (2 m, 4 m, 6 m, and 8 m bgs); or five screens (2 m, 3 m, 4 m, 5 m and 6 m bgs). Wells were spaced in ~1-m intervals around the injection location and then every 2 m, from 4 m to 10 m in the direction of groundwater flow (Figure 1b and 1c). In general, it is inevitable that sampling will influence flow paths in a groundwater system, particularly when there are 122 depth discrete sample points in an aquifer volume of ~350 m^3 (i.e. a high density of sampling points). However, the depth-discrete multilevel system with small diameter tubing (and low

volumes of groundwater extracted) was designed to minimize sampling-induced mixing of groundwater from different depths and to reduce any influence on the natural flow regime.

2.4 Analyses

Groundwater samples were collected from multi-level wells before, during and after (up to 700 days post injection) the introduction of natural gas into the aquifer. In addition to presenting previously unpublished geochemical and microbial data, this manuscript introduces new dissolved gas concentration and stable carbon isotope ratio data for samples from days 500 and 700, beyond those from Cahill et al. (2018).

Select field parameters were measured using a multi-parameter sonde and flow-through cell (Manta 2, Eureka Water Probes) supplied by a peristaltic pump at a flow rate of 40 to 50 mL min^{-1}. Measurements included EC (±1 μS cm^{-1}), pH (± 0.1), temperature (± 0.02 °C) and $O_{2(aq)}$ (± 0.02 mg L^{-1} for low $O_{2(aq)}$ range). The instrument was calibrated prior to each sampling campaign as per the manufacturer's guidelines. The EC meter was calibrated with a 1413 μS standard solution and pH was calibrated with pH 7 and 10 buffer solutions. The instrument was equipped with an optical $O_{2(aq)}$ sensor, known for very low drift in the field. The sonde auto-compensates for temperature (based on inbuilt temperature measurements for the sample). Dissolved gas samples were taken by submerging 40 mL volatile organic analysis vials in a beaker of sampled water immediately after sample collection and sealing the vials with septa caps leaving no headspace. Samples were stored upside down (to minimize potential gas exchange through the cap) at 4 °C and analyzed for $CH_{4(aq)}$, $C_2H_{6(aq)}$, $C_3H_{8(aq)}$, $CO_{2(aq)}$, and $N_{2(aq)}$ typically within 7 days, but no longer than 4 weeks after collection to minimize microbially mediated reactions in samples that were not treated with a biocide. The static headspace equilibrium technique

(Kampbell et al., 1989) was used to separate dissolved gases from water before analysing gas concentrations on a Bruker 450 Natural GC with measurement uncertainties of ± 5 % of the analyte. Although dissolved gas sampling with a peristaltic pump and the semi-open sampling method can result in degassing, appropriate steps were taken to minimize gas loss (e.g. low pumping rates and short tubing lengths). Due to the possibility of degassing, dissolved gas concentrations reported here should be considered conservative and might be higher in–situ. However, potential loss of dissolved gases does not interfere with the interpretations and conclusions of this manuscript, which mainly focus on changes in groundwater chemistry related to major ion and trace element concentrations, microbial community profiling, and stable carbon isotope ratios.

Samples for major and minor cations were filtered (0.45 µm cellulose acetate filters) and acidified (concentrated HNO_3) in the field and stored at 4 °C until analyses. Samples were analyzed on an Agilent 8800 Inductively Coupled Plasma Triple Quad Mass Spectrometer using the NIST SRM 1640a (Trace Elements in Natural Water) and CALA CO2A elements (full range) in water (Proficiency Testing Program) standards for QC/QA. Measured concentrations were within 5 % of the certified values (see Table S3 for detection limits). Samples for major anions (Cl^-, NO_3^- and SO_4^{2-}) were collected unfiltered and concentrations were determined using a Dionex ICS 2000 ion chromatograph (Dionex Corporation). A 25 µL aliquot of each sample was injected onto an Ion Pac AS18 anion column (Dionex Corporation) and then separated by isocratic elution using 35 mM potassium hydroxide, a flow rate of 1 mL min^{-1}, and a column temperature of 30 °C. Analytical precision and accuracy for anion analysis was ± 5 %. Alkalinity was determined in the field (by Gran titration) for selected samples.

Samples for analysis of stable carbon isotope ratios ($^{13}C/^{12}C$) of $CH_{4(aq)}$ and $CO_{2(aq)}$ were obtained by piercing the septa of pre-evacuated 125 mL glass vials that were filled by submersing them into a continuously filling sample container. Vials were treated with 20 µL of a biocide (mercuric chloride [$HgCl_2$]). The samples were stored at 4 °C prior to analysis using the static headspace equilibrium technique (Kampbell et al., 1989) to separate dissolved gases from water. Subsequently, headspace gas was injected into a gas chromatograph (GC) and carbon isotope ratios of $CO_{2(aq)}$ and $CH_{4(aq)}$ (after conversion to $CO_{2(aq)}$ and cryo-focussing) were determined with a ThermoFisher MAT 253 isotope ratio mass spectrometer (IRMS) coupled to a Trace GC Ultra + GC Isolink (ThermoFisher) at the Isotope Science Laboratory at the University of Calgary (Alberta, Canada). Carbon isotope ratio measurements of $CO_{2(aq)}$ were bracketed and normalized using two calibration gases with widely different $\delta^{13}C$ values (Oztech -3.6 and -48 ‰) that were anchored against international reference materials. For $CH_{4(aq)}$, additional reference gases from Scott ($\delta^{13}C$ of -69 and -25 ‰) and Isometric ($\delta^{13}C$ of -67, -38 and -24 ‰) were used to ensure complete conversion of $CH_{4(aq)}$ to $CO_{2(aq)}$ prior to mass spectrometric analyses and accurate $\delta^{13}C$ values for $CH_{4(aq)}$. Results are reported in the internationally accepted delta ($\delta^{13}C$) notation (in ‰) relative to VPDB with a precision better than ± 0.5 ‰ and ± 0.3 ‰ for $\delta^{13}C$ values of $CH_{4(aq)}$ and $CO_{2(aq)}$, respectively.

2.5 Geochemical Modeling

Geochemical modeling was conducted with Phreeqc Interactive (Version 3.4.0-12927 using the wateq4f database) to quantitatively evaluate water chemistry data with a focus on mineral solubility controls and to bracket hydrogeochemical changes. To determine saturation states for

select mineral phases at 2 m, 6 m, and 8 m bgs, speciation calculations were performed based on hydrogeochemical conditions (major ions, alkalinity, pH and temperature) before, during, and after injection from groundwater collected in a well near the injection location (M7, Table S4). Oxides containing oxidized forms of Fe and Mn were not included in the modeling due to uncertainties in aqueous redox equilibria.

Typically, hydrodynamic dispersion does not cause extensive mixing of groundwater and solutes in an aquifer. However, injection of free-phase gas could invoke mixing in two ways: 1) gas partitioning between dissolved gases present in the groundwater and gases constituting the free-phase injected gas and; 2) entrainment of deeper groundwater with upwards-migrating free-phase gas to shallower depths. Geochemical modeling was used to investigate the extent and impacts of these mixing processes along with CH_4 oxidation. To bracket the range of effects on pH and associated hydrogeochemical changes, all gas partitioning and reaction path simulations were performed with and without calcite equilibration.

The injected natural gas contained small amounts of $O_{2(g)}$ and $CO_{2(g)}$ (0.05 % and 0.8 %, respectively). Therefore, gas partitioning simulations were performed to assess pH and hydrogeochemical changes associated with $O_{2(g)}$ and $CO_{2(g)}$ dissolution into groundwater and, subsequent $CH_{4(aq)}$ oxidation by $O_{2(aq)}$. For these simulations, a gas phase mimicking the composition of the simulated natural gas injected during the field experiment (only containing CH_4, N_2, and either O_2 or CO_2) was introduced to baseline groundwater from M7 (Table S4 and Table S5). Natural gas constituents C_2H_6 and C_3H_8 were included in the initial analysis, but were not further considered since their presence had no noticeable impact on groundwater pH. When present, $O_{2(aq)}$ was allowed to oxidize $CH_{4(aq)}$, while $CH_{4(aq)}$ oxidation by other electron acceptors, such as SO_4^{2-} or NO_3^-, was excluded from these simulations. Gas partitioning

simulations were completed for 2 m, 6 m, and 8 m depths starting with baseline conditions from M7 for major ions, alkalinity, pH and temperature (Table S4). Gas phase pressures were fixed, dependent on the depth below the water table and, an initial water:gas volume ratio of 1:1 was assumed.

Our second mixing hypothesis was that deep groundwater could be entrained during the upward migration of the injected free phase gas and be displaced into shallower groundwater. To investigate the potential impacts caused by mixing of the displaced deep groundwater with shallower groundwater, Phreeqc simulations were performed where groundwater from depths of 2 m and 6 m, as well as 6 m and 8 m were mixed. For these simulations average baseline conditions for groundwater collected at M7 (Table S4) from depths of 2 m and 6 m, as well as 6 m and 8 m were mixed at ratios ranging from 0.1 to 0.9.

Geochemical changes in groundwater related to $CH_{4(aq)}$ oxidation with select electron acceptors (Table S1) were evaluated through reaction path simulations. Baseline groundwater from M7 (Table S4) was titrated with $CH_{4(aq)}$ (1.3 mmol L^{-1}) to mimic the injection of CH_4 present in the natural gas. Over 20 steps, one electron acceptor was isolated to react with the injected CH_4. Redox-active species not directly targeted in the simulations were decoupled to avoid the enforcement of unwanted redox equilibria complicating interpretation of the results (Table S4). The initial concentration of the electron acceptors was defined using baseline conditions at each depth from which groundwater was obtained (Table S4).

2.6 Microbial Community Profiling

Microbial biomass was collected from groundwater as described in Kenward et al. (2018). Environmental DNA was extracted from recovered biomass using DNeasy PowerSoil Kit (Qiagen) as per manufacturer's instructions. Resulting DNA was stored at -20 ^{o}C. Quantification was conducted using the PicoGreen® Assay (Invitrogen) for dsDNA (Singer et al., 1997), measured on a TECAN™ M200 (excitation at 480 nm and emission at 520 nm) (Table S6). Purity and quality of DNA was assessed based on ratios for A_{260}/A_{280} measured using a NanoDrop® ND-1000 spectrophotometer (Thermo Scientific). The V4-V5 region of the small subunit rRNA gene was amplified and sequenced, and the resulting sequence information processed using standard bioinformatic analyses to generate microbial community composition profiles (see SI Section 1 for details).

3. Results and Discussion

3.1. Baseline conditions

Prior to natural gas injection, $CH_{4(aq)}$ concentrations were naturally very low at all depths (ranging from 0.0001 to 0.02 mmol L^{-1}, Table S7). Stable carbon isotope analyses indicated a microbial origin of CH_4 with $\delta^{13}C$ values as low as -80 ‰ but also signs of $CH_{4(aq)}$ oxidation resulting in $\delta^{13}C$-CH_4 values as high as -47 ‰. Average $CO_{2(aq)}$ increased with depth, up to 2.5 mmol L^{-1} at 8 m bgs. Baseline $\delta^{13}C$-CO_2 values of -21 ‰ were measured at 2 m and 5 m depths. Dissolved N_2 varied over depth with concentrations ranging from 0.2 to 0.7 mmol L^{-1} (Table S7).

Two distinct hydrogeochemical zones were observed within the 8 m thick aquifer: an upper zone with fresh water and low TDS and hence EC (from water table to ~7 m depth) and, a thin zone at the base of the aquifer containing water with higher EC (8 m to 9 m depth).

Groundwater in the lower zone (8 m to 9 m depth) remains affected by the leachate from the construction waste landfill, as reported by McFarlane et al. (1983), as discussed in Section 2.1.

A shallow water table, as at our field site (~ 1 m bgs), can lead to incomplete oxidation of dissolved organic carbon (DOC) in the vadose zone. As a result, recharging groundwater through the vadose zone introduced DOC into the shallow aquifer (i.e. 2 m to 4 m bgs). Subsequent oxidation of DOC in the shallow aquifer caused mildly reducing conditions and low $O_{2(aq)}$ concentrations (< 0.01 mmol L^{-1}) under baseline conditions. Deeper in the aquifer (6 m to 8 m depths), $O_{2(aq)}$ concentrations decreased below the limit of detection (< 0.001 mmol L^{-1}, not shown), due to stronger reducing conditions caused by higher DOC content in the landfill leachate. Lower pH values (as low as 6.7 pH units) and higher alkalinities (up to 7.7 meq L^{-1}) were observed 6 m to 8 m bgs. However, pH was in general circumneutral at all depths (Table S7). The fresh groundwater in the upper zone (2 m to 6 m) was characterized by lower EC values (324 to 795 µS cm^{-1}) than in the deeper aquifer (1086 to 2433 µS cm^{-1} at 8 m bgs, Table S7). Elevated EC 8 m bgs is attributed to the higher concentrations of Cl^-, SO_4^{2-}, Ca^{2+}, Fe^{2+}, Mg^{2+}, Na^+ and H_4SiO_4 (Table S8). In general, there was variability in the baseline ranges of major and minor cation and anion concentrations. However, the ranges were comparable between shallow depths (2 m to 6 m) and higher 8 m bgs (Tables S8 and S9).

3.2. Evolution of dissolved gases

During and following injection, a strong correlation was observed for groundwater concentrations of $CH_{4(aq)}$ with $C_2H_{6(aq)}$ and $C_3H_{8(aq)}$ (correlation coefficients > 0.9, Cahill et al., 2018). The evolution of $CH_{4(aq)}$ is therefore representative for the behavior of all dissolved hydrocarbons. Cahill et al. (2018) provides a detailed description on the evolution of dissolved

gases; however, only up to day 300 of the experiment. In general, higher silt and clay contents between 2.5 m and 4 m bgs (Steelman et al., 2017) affected GM and led to greater average $CH_{4(aq)}$ concentrations during and after injection (>0.006 mmol L^{-1}) at 2 m, 6 m, and 8 m bgs compared to those monitored directly above the lower permeability lenses (e.g. 4 m bgs, Figure S1). Horizons at 2 m, 6 m, and 8 m depth are thus most suitable to assess potential impacts of fugitive CH_4 on long-term hydrogeochemical changes. Dissolved gas concentration trends at individual monitoring locations (M1-M32) were similar to trends for composite dissolved gas concentrations representing averages of all locations for each respective depth. Spatially averaged concentrations values for dissolved gases are therefore used to document long-term temporal changes at depths of 2 m, 6 m, and 8 m over a larger representative area of aquifer.

For the entire duration of monitoring (i.e. up to 700 days after start of injection), average $CH_{4(aq)}$ remained above baseline levels at depths of 2 m, 6 m, and 8 m (Figure 2). During active injection (day 0 to 72), $CH_{4(aq)}$ fluctuated at all depths with random events that led to marked increases in $CH_{4(aq)}$ concentrations at depth. Elevated concentrations at 2 m and 6 m led to lateral GM in the direction of groundwater flow and down gradient of the injection screens (Figure 2 and S1). At 2 m depth, the greatest increase in average $CH_{4(aq)}$ occurred from day 7 to 14, rising from 0.04 to 0.2 mmol L^{-1}, after which concentrations remained > 0.2 mmol L^{-1} to day 700. At 6 m bgs, the greatest increase in average $CH_{4(aq)}$ was from 0.003 mmol L^{-1} on day 14 to 0.2 mmol L^{-1} on day 28, after which concentrations remained elevated (>0.3 mmol L^{-1}) until day 300 (Figure 2). At 8 m bgs, average $CH_{4(aq)}$ increased on day 21 and remained >0.03 mmol L^{-1} until day 127. Episodic increases in $CH_{4(aq)}$ can be attributed to CH_4 dissolution following gas phase breakthrough driven by pore scale heterogeneities. Although the Borden aquifer is primarily comprised of fine sand, a detailed analysis of grain-size distribution at the field-site revealed

variations in grain size with laminations containing higher contents of silts and clay within fine sand layers. Lower permeability layers within the fine sand were identified between 2.5 m and 4 m bgs and from ~7.5 m to 9 m bgs. Between these layers were more coarse and medium sands containing some pebbles within the fine sand (Steelman et al., 2017). Due to buoyancy forces, gas phase CH_4 accumulated below the capillary barriers containing increased fine sand, silt and clay contents, until overcoming the entry pressure for breakthrough. Gas breakthrough resulted in dissolution of CH_4 in the overlying layers and/or migration to the vadose zone and atmosphere (Cahill et al., 2018; Forde et al., 2018; Steelman et al., 2017). Surface efflux and soil gas measurements demonstrated that CH_4 was intermittently released to the atmosphere due to episodic gas breakthrough from the saturated zone (Forde et al., 2018).

At all depths, maximum $CH_{4(aq)}$ concentrations were observed shortly after the injection stopped (day 77 to 113, Figure 2 and S1). The increase in concentrations is due to the loss of external (gas injection) pressure that had enabled the free phase gas buoyancy forces to overcome capillary forces. When injection stopped, free phase gas became trapped in place and inflowing groundwater promoted dissolution of gas bubbles. Dissolved CH_4 remained in the aquifer up to day 700 where $CH_{4(aq)}$ concentrations were the highest at 2 m depth (average of 0.2 mmol L^{-1} and up to 0.6 mmol L^{-1}), followed by concentrations at 6 m (average of 0.01 mmol L^{-1} and up to 0.02 mmol L^{-1}) and 8 m (average of 0.008 mmol L^{-1} and up to 0.2 mmol L^{-1}) depths (Figure 2). Although $CH_{4(aq)}$ began to decrease towards the end of the experimental monitoring period, concentrations were still above baseline. Persistence of elevated $CH_{4(aq)}$ on day 700 (up to 0.6 mmol L^{-1} 2 m bgs) is indicative of continued dissolution of entrapped gas. However, the decline in concentrations also suggest the occurrence of oxidation (see Section 3.3), flushing and/or dilution.

Average $CO_{2(aq)}$ concentrations at depths of 2 m and 6 m were above baseline (by 0.2 mmol L^{-1}) during injection, but then declined until the end of monitoring (day 700), with the exception of an increase on day 500 (Figure 2). At 2 m bgs, the greatest increases in $CO_{2(aq)}$ (to 0.7 mmol L^{-1}) were observed at the same location (M7) where some of the highest $CH_{4(aq)}$ concentrations were detected (up to 1.8 mmol L^{-1}). The same correlation of locations with highest $CO_{2(aq)}$ and elevated $CH_{4(aq)}$ was observed at 6 m bgs. The increase in $CO_{2(aq)}$ may be due to CH_4 oxidation. At 8 m depth, aside from day 14, $CO_{2(aq)}$ slightly decreased below baseline (by up to 0.6 mmol L^{-1}). The decline in $CO_{2(aq)}$ can be attributed to stripping of CO_2 due to the natural gas injection. Stripping likely only occurred at 8 m due to the fact that this sampling depth is closer to the injection well (at 9 m) than the 6 m and 2 m sampling ports, and is thus more directly influenced by the natural gas release.

Similar to the stripping of $CO_{2(aq)}$ at 8 m depth, $N_{2(aq)}$ concentrations decreased below baseline values at all depths during and shortly after the injection (day 0 to 120). Stripping of $N_{2(aq)}$ further supports the existence of a dynamic system with free phase CH_4 migration. However, towards the end of the monitoring period, $N_{2(aq)}$ concentrations increased above baseline from 0.6 mmol L^{-1} to 2.4 mmol L^{-1} at 2 m bgs (Figure 2). Enrichment of $N_{2(aq)}$ concentrations at late time may be indicative of near complete CH_4 dissolution, caused by flushing with CH_4-free groundwater and possibly enhanced by $CH_{4(aq)}$ oxidation. Both CO_2 and CH_4 have higher solubilities than N_2 (effectively 33.6 mmol L^{-1}, 1.4 mmol L^{-1}, and 0.6 mmol L^{-1}, respectively at 298 K and 10^5 Pa). As a result, CH_4 and CO_2 preferentially dissolved from entrapped gas into the inflowing groundwater post injection. Simultaneously, $N_{2(aq)}$ partitioned into the entrapped gas bubbles due to the naturally higher $N_{2(aq)}$ in the inflowing groundwater, and thereby leading to an increase of N_2 in the residual gas bubbles. The residual gas bubbles

became progressively N_2 enriched due to CH_4 and CO_2 preferentially dissolving into CH_4-free and CO_2-poor ingressing groundwater, flushing and oxidation. Enrichment of N_2 in entrapped gas provided a driving force for N_2 dissolution into groundwater, explaining the observed elevated $N_{2(aq)}$ concentrations at late time. A similar observation was also made in an aquifer experiment in Bitterfeld, Germany (Balcke et al., 2011). Denitrification may provide an alternative source for N_2, particularly at 6 m depth, where NO_3^- concentrations slightly decreased. However, N_2-enrichment at 8 m bgs coincided with a rise in NO_3^- concentrations, and NO_3^- was generally below detection at 2 m depth (see Section 3.3 and Table S10), implying that dissolution from N_2-enriched gas bubbles provides a more likely explanation. Although N_2 stripping can be associated with fugitive GM (Cahill et al., 2018; Larson et al., 2018), we show here that enrichment in $N_{2(aq)}$ can also be expected post wellbore leakage. Particularly, N_2 enrichment could be used as an indicator for substantial or near-complete removal of free-phase CH_4 from an aquifer.

3.3. Occurrence and extent of fugitive methane oxidation

3.3.1. Stable carbon isotope ratios

Natural attenuation of $CH_{4(aq)}$ through oxidation depends on catalysis by the resident microbial community, which couples $CH_{4(aq)}$ oxidation to the reduction of available terminal electron acceptors (Table S1) (Röling and van Verseveld, 2002; Scow and Hicks, 2005). Microbes preferentially oxidize $CH_{4(aq)}$ containing the light isotope ^{12}C resulting in a progressive enrichment of the heavier isotope ^{13}C in the remaining $CH_{4(aq)}$ (Barker and Fritz, 1981; Whiticar and Faber, 1986). Therefore, $\delta^{13}C$-CH_4 values higher than the injected natural gas (-42 ‰) can

be attributed to $CH_{4(aq)}$ oxidation. From day 0 to 300, only eight of 114 samples displayed ^{13}C enrichment compared to the injected CH_4 (Cahill et al., 2018). These samples were all from 8 m depth with $\delta^{13}C\text{-}CH_4$ values ranging from -40 ‰ to -33 ‰ and associated $CH_{4(aq)}$ concentrations of 0.05 and 0.01 mmol L^{-1}, respectively. From day 300 to 700, 56 of 132 samples from all depths (except 3 m) had $\delta^{13}C\text{-}CH_4$ values more ^{13}C-enriched than that of injected CH_4 ranging from -40 ‰ to +18 ‰ with associated $CH_{4(aq)}$ of 1.0 and 0.002 mmol L^{-1}, respectively (Figure 3a). The greatest ^{13}C-enrichment in remaining $CH_{4(aq)}$ in groundwater throughout the entire experiment was observed at 8 m depth on day 500 with $\delta^{13}C\text{-}CH_4$ values ranging from -15 ‰ to +18 ‰ and $CH_{4(aq)} < 0.006$ mmol L^{-1} (n = 9) (Figure 3a). The injected gas had a gas dryness (ratio of methane [C_1] to ethane [C_2] plus propane [C_3]) of ~23.4. From day 300 to 700 , 53 of 64 samples retained this thermogenic signature (Figure 3b). Samples that were not enriched in ^{13}C were either similar to the isotopic signature and concentration of background $CH_{4(aq)}$ (e.g. -67 ‰ and $CH_{4(aq)}$ of 0.006 mmol L^{-1}) or, at higher concentrations, most $\delta^{13}C\text{-}CH_4$ values were only slightly lower than that of the injected gas (e.g. -43 ‰ and $CH_{4(aq)}$ of 0.6 mmol L^{-1}). Values where $\delta^{13}C\text{-}CH_4$ was ~~lighter~~ more negative than the injected gas could be due to preferential fractionation of the light isotope (^{12}C) with diffusive migration (Chanton, 2005; Egger et al., 2015) and/or, mixing of background and injected CH_4 associated with gas partitioning between natural groundwater and injected gas. The greatest ^{12}C-enrichment in $CH_{4(aq)}$ was observed at 2 m depth, located vertically farthest away from the injection points at 9 m and 4.5 m, consistent with C-isotope fractionation of $CH_{4(aq)}$ due to diffusive migration away from the injection locations (Figure 3). Two end member mixing calculations of background $\delta^{13}C\text{-}CH_4$ (-47 ‰ to -80 ‰) with injected $\delta^{13}C\text{-}CH_4$ (-42 ‰) led to $\delta^{13}C\text{-}CH_4$ values between -42 ‰ and -45 ‰. Therefore, samples with $\delta^{13}C\text{-}CH_4$ values lower than -45 ‰ and higher $CH_{4(aq)}$ concentrations are likely

associated with both fractionation due to diffusive transport and C-isotope mixing with background CH_4. Overall, the much higher occurrence of ^{13}C-enrichment in $CH_{4(aq)}$ across the aquifer from day 300 to 700 indicates that the extent of $CH_{4(aq)}$ oxidation substantially increased with time.

From day 50 to 700, $\delta^{13}C\text{-}CO_2$ decreased from baseline of -21 ‰ to values between -22 ‰ to -24 ‰ (Figure S2). Enrichment of ^{12}C in $CO_{2(aq)}$ and ^{13}C in $CH_{4(aq)}$ implies $CH_{4(aq)}$ oxidation, primarily from day 300 to 700. Changes in $\delta^{13}C\text{-}CO_2$ were much smaller (at most 5 ‰) than those for $^{13}C\text{-}CH_4$ due to the high total inorganic carbon (TIC) content (up to 13 mmol L^{-1}) of background groundwater. High TIC minimizes changes in $\delta^{13}C\text{-}CO_2$ with $CH_{4(aq)}$ oxidation and leads to relatively constant $CO_{2(aq)}$ concentrations, as observed throughout the experiment at each depth (Figure 2). The variations of stable carbon isotope ratios over time and depth may imply a dynamic evolution of microbially mediated processes (aerobic versus anaerobic) involved in $CH_{4(aq)}$ oxidation.

3.3.2. Microbial community profiling

Focusing on the most recent data from day 700, microbial community profiling revealed a relatively diverse assemblage of microorganisms (Figure S3) including taxa related to those with known metabolic potential for aerobic $CH_{4(aq)}$ oxidation, as well as a single taxon related to *Candidatus methylomirabilis*, which is best known for its capacity to couple $CH_{4(aq)}$ oxidation to denitrification (Figure S4). At day 700, the microbial community was comprised of between 441 and 1376 operational taxonomic units (OTU, 97 % similarity) (SI Section 2) (Figure S5 and S6). From day 0 to 700, 46 taxa were identified related to organisms previously implicated in coupled

C, $O_{2(aq)}$, N, Fe, and S cycling as well as $CH_{4(aq)}$ and methylated compound metabolism (Figure S4). The most abundant organisms were related to those with known metabolic potential for methylotrophy, a diverse group of micro-organisms specialized on oxidizing reduced single carbon compounds, providing indirect evidence for $CH_{4(aq)}$ oxidation (Figure S4). Organisms with potential for methanotrophy or NO_3^- respiration were most abundant between 2 m and 4 m depths and their abundances increased rapidly with natural gas injection. Microorganisms known as SO_4^{2-} reducers were also present, predominantly post injection at 8 m depth within the sulfate-rich groundwater affected by landfill leachate. Although organisms related to SO_4^{2-} reducers were present at relatively low abundances, this group of microorganisms showed a relatively high degree of diversity (Figure S4, SI Section 2). Figure 4 also indicates that the ingrowth of organisms related to SO_4^{2-} reducers proceeded relatively slowly in comparison to those related to methanotrophs and denitrifiers with the highest abundances and diversity seen at day 700. Organisms known to reduce Fe(III) were also present, but clear chemical evidence for iron respiration was sparse (Figure S4). Although the strongest isotopic evidence for $CH_{4(aq)}$ oxidation occurred post injection, the microbial community adapted relatively quickly (first evidence on day 45) with a persistent perturbation to the composition. The diversity in organisms is comparable to previous analyses of shallow subsurface microbial communities (Gulay et al., 2016; Sang et al., 2018; Unno et al., 2015; Vosin et al., 2018) and this likely reflects microbial community metabolism through both aerobic $CH_{4(aq)}$ oxidation and anaerobic respiration. The development of a microbial community capable of aerobic CH_4 oxidation could have been initiated through dissolution of $O_{2(g)}$ introduced with the injected simulated natural gas, particularly in the anoxic environment at 8 m depth. Microbial evidence for aerobic $CH_{4(aq)}$ oxidation in an anoxic environment does not preclude anaerobic $CH_{4(aq)}$ oxidation. Rather, it

implies a complex interaction among micro-organisms, for which the analysis was beyond the scope of this paper.

3.3.3. Redox indicator species

Throughout the experiment average changes in concentrations of redox indicator species were subtle (Figure 4, typically <1 mmol L^{-1}), and did not provide clear evidence for the mechanism(s) of $CH_{4(aq)}$ oxidation. Utilization of the various electron acceptors has been shown to affect groundwater pH in characteristic ways. Typically, pH decreases during aerobic respiration, increases with Fe(III)- and Mn(IV)-oxide reduction, and changes minimally during denitrification and bacterial SO_4^{2-} reduction (Appelo and Postma, 2004; Mayer et al., 2001). To further evaluate the contribution of the various electron-accepting processes to $CH_{4(aq)}$ oxidation, reaction path simulations with Phreeqc were performed by titrating $CH_{4(aq)}$ into baseline groundwater at various depths (Table S5). For each simulation, redox reactions were restricted to a single electron acceptor to isolate its contribution to pH changes. Simulation results indicated very limited pH changes consistent with those observed at the field site (<0.3 pH units) for $CH_{4(aq)}$ oxidation coupled to aerobic respiration, denitrification and bacterial SO_4^{2-} reduction. However, the results also suggested that substantial Fe(III) and Mn(IV)-reduction would lead to marked increases in groundwater pH (>0.3 pH units), not observed in our experiment. These site-specific results confirm previous findings (Appelo and Postma, 2004; Mayer et al., 2001). However, slight increases of Fe^{2+} and Mn^{2+} concentrations could indicate that a minor amount of Fe(III) and Mn(IV) reduction did occur. Lower pH values despite the occurrence of reductive dissolution could be due to Fe^{2+} and Mn^{2+} sorption and deprotonation. Reactive transport

modeling of geochemical processes in a hydrocarbon contaminant plume in the Bemidji aquifer, United States of America, demonstrated that Fe^{2+} adsorption coupled with deprotonation provided a pH buffer to reduce secondary groundwater impacts (Ng et al., 2015). Nitrate and SO_4^{2-} concentrations fluctuated in unexpected ways; at times increasing above baseline concentrations indicating no consistent evidence for $CH_{4(aq)}$ oxidation coupled with the reduction of these electron acceptors (Figure 4 and Table S10). The fluctuation in redox indicator species indicates that their natural variability was enhanced by other mechanisms beyond $CH_{4(aq)}$ oxidation, over-printing changes that could otherwise be attributed to $CH_{4(aq)}$ oxidation. These changes are likely associated with physical processes occurring as a result of natural gas injection (see Section 3.4).

3.4. Hydrogeochemical changes as a consequence of fugitive gas migration and methane oxidation

3.4.1 Evolution of EC and pH

The natural gas injection led to perturbations of aqueous geochemistry as evidenced by changes in EC and pH. From day 0 to 300, EC ranged from 240 μS cm^{-1} (at 2 m bgs) to 844 μS cm^{-1} (at 6 m bgs), and generally increased at 2 m and 6 m depths during injection (Figure S7). There were four events when EC increased >100 μS cm^{-1} above baseline at depths of 2 m and 6 m (days 21, 28, 63 and 70) (Figure S7). After day 300, EC returned to baseline values in groundwater at 2 m and 6 m depths, ranging from 166 μS cm^{-1} (at 2 m) to 559 μS cm^{-1} (at 6 m). The observed sporadic increases in EC can be attributed to increases in SO_4^{2-} (Figure 4) and other major ions, particularly Na^+ and Cl^- (Figure 5). When EC increased, the ion composition at 2 m bgs was similar to baseline groundwater at 6 m bgs and, the groundwater ion composition at 6 m bgs was

close to the baseline composition 8 m bgs (Figure 6a). The similarities between groundwater compositions from 6 m bgs and 8 m bgs (Figure 6) suggests that the landfill leachate at the base of the aquifer (8 m to 9 m depth) was entrained and pulled upward during episodic gas breakthroughs, contributing to temporary increases in EC (Figure S7).

Natural gas injection at 9 m depth led to an upward displacement of landfill leachate contaminated groundwater with TDS concentrations at least twice as high as in shallower uncontaminated groundwater. As gas migrated upward, driven by buoyancy forces, the entrained leachate impacted water-filled pore spaces and mixed with fresher groundwater. Mixing lines (modeled with Phreeqc) for SO_4^{2-} and Cl^- involving groundwaters from 2 m and 6 m depths, as well as 6 m and 8 m depths (Figure 6b) support the upward migration and mixing of deep more acidic water with shallow groundwater. Mixing led to a temporary rise of ion concentrations and contributed to the decrease in pH at depths of 2 m and 6 m from day 0 to 300 (Figure S8 and Table S10). Throughout the experiment, pH at depths of 2 m, 6 m and 8 m fluctuated around 7 by up to ± 0.3 pH units (Table S10). In the short-term (day 0 to 300), the average pH decreased in groundwater at depths of 2 m and 6 m by 0.3 and 0.1 pH units, respectively. Phreeqc mixing simulations demonstrate that a pH decrease by 0.2 pH units can be obtained in the shallower groundwater by entraining and mixing groundwaters from 6 m depth and 2 m depth (or groundwaters from 8 m depth and 6 m depth) at a 1:9 (shallow:deep groundwater) ratio. However, for both scenarios, the pH change is restricted to 0.1 pH units for a 1:1 mixing ratio, suggesting that entrainment of deeper water alone cannot fully explain the observed pH decreases. An additional process that can contribute to the observed pH decreases is the dissolution of $CO_{2(g)}$ present in the natural gas at low concentrations. Gas partitioning simulations with Phreeqc showed that equilibrating natural gas containing 0.8 % $CO_{2(g)}$ at a 1:1

volume ratio with baseline groundwater causes a pH decrease by up to 0.1 pH units at 2 m and 6 m depths (Table S5). As discussed above, aerobic $CH_{4(aq)}$ oxidation is another process that can cause pH to decline. Aerobic $CH_{4(aq)}$ oxidation may be driven by $O_{2(aq)}$ present in shallow groundwater prior to injection or a small fraction of O_2 that was present in the injected gas (0.05 % O_2). Gas partitioning simulations accounting for the O_2 in the natural gas and allowing for its reduction by $CH_{4(aq)}$ oxidation indicate only a small pH decline restricted to <0.02 pH units at depths 2 m and 6 m due to this process (Table S5). The negligible change in pH implies that the presence of O_2 in the injected gas was of minor importance to the redox environment, but may have contributed to the growth of organisms with known potential for methanotrophy (Figure S4). Although it is not possible to identify a specific process responsible for the observed pH decreases, a combination of entrainment and mixing, $CO_{2(g)}$ dissolution, and $CH_{4(aq)}$ oxidation likely caused the decline of pH in groundwater at 2 m and 6 m depth between days 0 to 300. It can be concluded that pH changes were minor (at times below measurement accuracy).

3.4.2. Distribution of major ions and trace elements

Major ion concentrations fluctuated over time, particularly during active injection. The greatest increases were observed for Ca^{2+}, Mg^{2+}, Na^{+} and H_4SiO_4 at 2 m, 6 m and 8 m depths, with less pronounced changes observed for Cl^{-} and K^{+} (Figure 5, Table S10). The initial rise in Ca^{2+} concentrations at all depths could be due to upwelling of higher TDS from deeper groundwater, possibly sustained by the occurrence of calcite dissolution buffering pH-decreases caused by various processes discussed above. Throughout the experiment, Ca^{2+} remained above baseline concentrations in groundwater at 2 m, 6 m and 8 m depths (Figure 5 and Table S10). Computed

saturation indices for groundwater from well M7 at depths of 2 m, 6 m, and 8 m demonstrate that groundwater remained near equilibrium with calcite throughout the experiment (Figure S9), confirming its reactivity and presence in the aquifer. Increases of Mg^{2+} and Na^{+} concentrations in groundwater may be due to upwelling of higher TDS groundwater from 8 m to 9 m depths in response to the natural gas injection and/or due to displacement from cation exchange sites by Ca^{2+} stemming from calcite and/or dolomite (for Mg^{2+}) dissolution (Figure 5 and Table S10). The increase in H_4SiO_4 concentrations can be attributed to dissolution of silicate minerals (e.g. amphiboles, feldspars, chlorite are all present in the Borden aquifer) as a result of the mild pH decrease. Geochemical speciation calculations for groundwater from well M7 also indicated that groundwater was undersaturated with respect to gypsum, dolomite, pyrochroite, rhodochrosite and amorphous silica (Figure S9), implying that these phases do not act as solubility controls for Ca^{2+}, Mg^{2+}, Mn^{2+}, and SO_4^{2-} ions. In general, changes in major ions were minor (Table S10) and most concentrations were trending back to baseline levels towards the end of the experiment (day 700, except H_4SiO_4).

A primary concern regarding GM into groundwater is the mobilization of trace elements through biogeochemical reactions induced by fugitive CH_4 (Vidic et al., 2013). The extent of trace element mobilization is a function of local aquifer geochemistry and sediment mineralogy. Changes in trace element concentrations were minor, fluctuating above and below baseline levels throughout the experiment. Displacement of water from 8 m to 9 m depths due to the gas injection may have contributed to an increase in trace elements at 2 m and 6 m depths (Figure 7). An additional potential explanation for increased trace element concentrations is their release due to cation exchange and surface complexation reactions associated with increases in major ions. Most trace elements started to decrease post injection, except for Al, As, Zn, and Cr, which were

still above baseline on day 700 (Figure 7). Similar to H_4SiO_4, increased Al concentrations were likely caused by the dissolution of silicate minerals, but concentration increases were limited as indicated by undersaturated conditions with respect to amorphous aluminum hydroxide [$Al(OH)_3(a)$] (Figure S9). While various mechanisms likely contributed to the fluctuation in trace elements, the exact processes were difficult to discern amongst the natural variability observed in the aquifer. It is possible that fluctuations in groundwater temperature affected concentrations of dissolved ions. However, groundwater temperature in the Borden aquifer is relatively constant around 10 °C at depths between 5 m to 9 m bgs (Allen-King et al., 1995; Arildskov and Devlin, 2000; Nielsen et al., 1996), implying that variations in concentrations are unlikely due to seasonal effects.

Although not a major mechanism for $CH_{4(aq)}$ oxidation, minor reductive dissolution of Fe and Mn-oxides did occur, as evidenced by the increase in Fe^{2+} and Mn^{2+} concentrations (Figure 4). Reductive dissolution reactions are well known to contribute to the release of trace elements due to the destruction of sorption sites (Appelo and Postma, 2004). In particular, mobilization of As poses major health risks even at low concentrations (EPA maximum contaminant level [MCL] is 0.13 μmol L^{-1}). On day 300 at 8 m depth, locations around the injection point (M5, M6, and M11) had groundwater with As concentrations above the EPA MCL, up to 0.20 μmol L^{-1} (Table S11). Aside from the samples at 8 m depth on day 300, all other samples (including baseline, Table S9) had As concentrations below the MCL (Figure 7). Although changes to the aquifer geochemistry were minor throughout our experiment, short-term and long-term trends associated with the natural gas injection and $CH_{4(aq)}$ oxidation, respectively, were evident.

3.5. Short and long-term biogeochemical evolution

We hypothesize that two biogeochemical stages progressively evolved as a consequence of the natural gas injection and subsequent $CH_{4(aq)}$ oxidation. First, in the short-term (day 0 to 300) groundwater geochemistry changed predominantly due to upwelling of deeper landfill leachate water with free phase GM. Minor changes were also associated with the introduced $CO_{2(g)}$ in the natural gas. Second, in the long-term (day 300 to 700) additional geochemical changes were observed in groundwater due to both aerobic and anaerobic (NO_3^- and SO_4^{2-} respiration) metabolisms at all depths (Figure 8).

Entrainment of deeper groundwater into shallower groundwater with subsequent mixing can be explained by buoyancy-driven vertical migration of injected natural gas, causing lateral and upward displacement of landfill leachate and groundwater around the injection zone (Figure 8a). The extent of this condition locally is masked by sampling scale/resolution. Enhanced mixing in groundwater has also been observed in air sparging studies due to the formation and collapse of gas channels during air injection (Heron et al., 2003; Kirtland and Aelion, 2000; Yang et al., 2005). A similar analogy can be made for our study where the formation and collapse of channels, as gas vented towards the atmosphere, created pathways for entrainment of deeper landfill impacted groundwater to migrate vertically and mix with shallower water (Figure 8a). The hydrogeochemical changes due to groundwater mixing were enhanced by disturbances from $CO_{2(g)}$ dissolution.

In the long-term, $CH_{4(aq)}$ oxidation progressed and, in some locations, approached completion between day 300 and 700, as evidenced by low residual concentrations and a strong ^{13}C enrichment in CH_4 (Figure 8b). However, geochemical impacts associated with $CH_{4(aq)}$ were minor, limited by carbonate mineral dissolution. Arsenic was the only trace element that exceeded drinking water standards for a short time period 8 m bgs. Few studies have constrained

$CH_{4(aq)}$ oxidation rates in the context of fugitive GM. In natural systems, $CH_{4(aq)}$ oxidation rates (both aerobic and anaerobic) can range widely from 10^{-2} to 10^{-8} g CH_4 L^{-1} day^{-1} (Roy et al., 2016). Higher oxidation rates require abundant presence of $O_{2(aq)}$, which was not the case in our study. The long-term results (day 300 to 700) suggest that for this small volume release experiment, oxidation led to natural attenuation of $CH_{4(aq)}$ but only subtle changes in aquifer geochemistry.

The assessment for fugitive CH_4 natural attenuation potential and magnitude of secondary groundwater impacts from degradation reactions remains an important topic of research. Previous field studies have demonstrated that fugitive CH_4 can persist in an aquifer for long periods of time (Schout et al., 2017; Wolfe and Wilkin, 2017). Schout et al. (2017) measured elevated $CH_{4(aq)}$ concentrations in an aquifer 50 years after a gas well blowout occurred. While our results demonstrate that $CH_{4(aq)}$ can be oxidized, they also suggest that the rate of oxidation in groundwater is low. These findings support previous studies that show CH_4 can persist if present as a free phase gas in high abundance (e.g. Schout et al., 2017) and under oxygen-limited conditions. Similar temporal scales have been reported for natural attenuation studies at organic and hydrocarbon contaminant release sites (Essaid et al., 2011; Scow and Hicks, 2005).

The rate and mechanism(s) of aquifer-specific fugitive CH_4 attenuation need to be constrained to characterize potential risks of GM. The hydrogeochemical impacts associated with fugitive gas invasion and CH_4 attenuation will further depend on the aquifer specific hydro-biogeochemistry, the magnitude and duration of gas leakage, and the composition of natural gas (i.e. $CO_{2(g)}$ content). The mineralogy of the Borden aquifer allowed for sufficient buffering to minimize hydrogeochemical impacts. However, this may not be the case for other sedimentary

basins with oil and gas development. Limited impacts are also due to the relatively small volume of injected gas in comparison to reported well blowouts which saw impacts > 500 m from the well (Kelly et al., 1985; Schout et al., 2017) and over an 11 km^2 area (Kelly et al., 1985). However, our controlled experiment demonstrated that hydro-biogeochemical changes due to fugitive GM can occur even on a small scale (aquifer volume and mass of gas released). The short- and long-term results emphasize the need for appropriate monitoring corroborated by site specific characterization involving: 1) aquifer hydro-biogeochemistry, lithology and mineralogy; 2) gas composition, rate of release and duration.

4. Conclusion

Simulated wellbore leakage through a natural gas injection led to vertical entrainment and mixing of deep, lower quality water with shallow, higher quality water within a surficial unconfined aquifer system. Upwelling of deep water transported major ions and trace elements into the shallower aquifer causing a deterioration in water chemistry. Geochemical changes in the groundwater were also caused by the addition of $CO_{2(g)}$ (0.8 %) and to a much lesser degree $O_{2(g)}$ (0.05 %) present in the simulated natural gas. Depending on the natural aquifer geochemistry, subsurface leakage of natural gas with elevated $CO_{2(g)}$ contents could have significant effects to the water chemistry, in particular due to more pronounced pH decreases. Although minor, the dynamic changes in groundwater chemistry during active injection demonstrate the need to better characterize processes induced by free phase fugitive GM from oil and gas wells. There is a potential for deep water with high TDS (e.g. saline) to be displaced by free phase GM, impacting water chemistry in shallow aquifers.

Post injection (up to 700 days) $CH_{4(aq)}$ persisted in groundwater, but stable carbon isotope ratios provided strong evidence for CH_4 attenuation by oxidation in parts of the aquifer. Microbial community profiling implied capacity for aerobic $CH_{4(aq)}$ oxidation, concomitant with anaerobic respiration of nitrate and SO_4^{2-}, and to a lesser extent Fe-oxides. Although fugitive GM impacts are aquifer specific, long-term changes in the Borden aquifer did show slight increases in trace elements. Throughout the experiment, pH variations and associated geochemical changes were limited by carbonate mineral dissolution. To fully delineate groundwater risks from fugitive GM, the mechanism(s) and rates of natural CH_4 attenuation need to be better constrained. The simulated release of natural gas into a shallow unconfined aquifer led to a persistent CH_4 groundwater plume with minor changes in major ions and trace elements associated with the gas injection and $CH_{4(aq)}$ oxidation. However, hydro-biogeochemical impacts from fugitive GM will be specific to the natural aquifer composition, baseline groundwater composition and the nature of the gas leakage.

Acknowledgements

This research was funded by an NSERC Strategic Partnerships Grant (SPG-P) Grant no. 463045-14 led by the University of Guelph. Further support through an NSERC Research Tools and Instrument (RTI) Grant and a CFI-LOF grant awarded to K.U. Mayer and a NSERC discovery grant to B. Mayer is gratefully acknowledged. We thank Michael Nightingale, Andreas Haggman, Bethany Ladd, Dylan Klazinga, Terri Cheung, Leon Halwa, and Alyssa Verdin for their field and laboratory assistance.

References

Amos, R.T., Bekins, B.A., Cozzarelli, I.M., Voytek, M.A., Kirshtein, J.D., Jones, E.J.P., Blowes, D.W., 2012. Evidence for iron-mediated anaerobic methane oxidation in a crude oil-contaminated aquifer. Geobiology 10, 506–517. https://doi.org/10.1111/j.1472-4669.2012.00341.x

Appelo, C.A.J., Postma, D., 2004. Geochemistry, Groundwater and Pollution. CRC Press. https://doi.org/10.1201/9781439833544

Balcke, G.U., Hahn, M., Oswald, S.E., 2011. Nitrogen as an indicator of mass transfer during in-situ gas sparging. J. Contam. Hydrol. 126, 8–18. https://doi.org/10.1016/j.jconhyd.2011.05.005

Ball, W.P., Buehler, C., Harmon, T.C., Mackay, D.M., Roberts, P.V., 1990. Characterization of a sandy aquifer material at the grain scale. J. Contam. Hydrol. 5, 253–295. https://doi.org/10.1016/0169-7722(90)90040-N

Barker, J.F., Fritz, P., 1981. Carbon isotope fractionation during microbial methane oxidation. Nature 293, 289-291. https://doi.org/10.1038/293289a0

Botner, E.C., Townsend-Small, A., Nash, D.B., Xu, X., Schimmelmann, A., Miller, J.H., 2018. Monitoring concentration and isotopic composition of methane in groundwater in the Utica Shale hydraulic fracturing region of Ohio. Environ. Monit. Assess. 190: 322. https://doi.org/10.1007/s10661-018-6696-1

Bordeleau, G., Rivard, C., Lavoie, D., Lefebvre, R., Malet, X., Ladeveze, P., 2018. Geochemistry of groundwater in the Saint-Edouard area, Quebec, Canada, and its influence on the distribution of methane in shallow aquifers. App. Geochem. 89, 92-108. https://doi.org/10.1016/j.apgeochem.2017.11.012

Burgess, W.G., Pinto, L., 2016. Preliminary observations on the release of arsenic to groundwater in the presence of hydrocarbon contaminants in UK aquifers. Mineral. Mag. 69, 887–896. https://doi.org/10.1180/0026461056950296

Butler, B.J., Barbaro, S.E., Crocker, F.H., Mayfield, C.I., 1997. Characterization of microbial populations of the borden aquifer. Geomicrobiol. J. 14, 253–268. https://doi.org/10.1080/01490459709378051

Cahill, A.G., Beckie, R., Ladd, B., Sandl, E., Goetz, M., Chao, J., Soares, J., Manning, C., Chopra, C., Finke, N., Hawthorne, I., Black, A., Mayer, K.U., Crowe, S., Cary, T., Lauer, R., Mayer, B., Allen, A., Kirste, D., Welch, L., 2019. Advancing knowledge of gas migration and fugitive gas from energy wells in northeast British Columbia, Canada. Greenh. Gases Sci. Technol. 9, 134-151. https://doi.org/10.1002/ghg.1856

Cahill, A.G., Jakobsen, R., 2013. Hydro-geochemical impact of CO2 leakage from geological storage on shallow potable aquifers: A field scale pilot experiment. Int. J. Greenh. Gas Control. 19, 678–688. https://doi.org/10.1016/j.ijggc.2013.03.015

Cahill, A.G., Marker, P., Jakobsen, R., 2014. Hydrogeochemical and mineralogical effects of sustained CO2 contamination in a shallow sandy aquifer: A field-scale controlled release experiment. Water Resour. Res. 50, 1735–1755. https://doi.org/10.1002/2013WR014294

Cahill, A.G., Parker, B.L., Mayer, B., Mayer, K.U., Cherry, J.A., 2018. High resolution spatial and temporal evolution of dissolved gases in groundwater during a controlled natural gas release experiment. Sci. Total Environ. 622–623, 1178–1192. https://doi.org/10.1016/j.scitotenv.2017.12.049

Cahill, A.G., Steelman, C.M., Forde, O., Kuloyo, O., Ruff, E.S., Mayer, B., Mayer, K.U., Strous, M., Ryan, C.M., Cherry, J.A., Parker, B.L., 2017. Mobility and persistence of methane in groundwater in a controlled-release field experiment. Nat. Geosci. 10, 289–294. https://doi.org/10.1038/ngeo2919

CCA, 2014. Environmental Impacts of Shale Gas Extraction in Canada: The Expert Panel on Harnessing Science and Technology to Understand the Environmental Impacts of Shale Gas Extraction. Council of Canadian Academies (CCA), Ottawa, Canada.

Chanton, J. P., 2005. The effect of gas transport on the isotope signature of methane in wetlands. Org. Geochem. 36, 753–768. https://doi.org/10.1016/j.orggeochem.2004.10.007

Christensen, T.H., Bjerg, P.L., Banwart, S.A., Jakobsen, R., Heron, G., Albrechtsen, H.J., 2000. Characterization of redox conditions in groundwater contaminant plumes. J. Contam. Hydrol. 45, 165–241. https://doi.org/10.1016/S0169-7722(00)00109-1

Cozzarelli, I.M., Schreiber, M.E., Erickson, M.L., Ziegler, B.A., 2016. Arsenic Cycling in Hydrocarbon Plumes: Secondary Effects of Natural Attenuation. Groundwater. 54, 35–45. https://doi.org/10.1111/gwat.12316

Darrah, T.H., Vengosh, A., Jackson, R.B., Warner, N.R., Poreda, R.J., 2014. Noble gases identify the mechanisms of fugitive gas contamination in drinking-water wells overlying the Marcellus and Barnett Shales. Proc. Natl. Acad. Sci. U.S.A. 111, 14076–14081. https://doi.org/www.pnas.org/cgi/doi/10.1073/pnas.1322107111

Dusseault, M., Jackson, R., 2014. Seepage pathway assessment for natural gas to shallow groundwater during well stimulation, in production, and after abandonment. Environ. Geosci. 21, 107–126. https://doi.org/10.1306/eg.04231414004

Dyck, W., Dunn, C.E., 1986. Helium and methane anomalies in domestic well waters in southwestern Saskatchewan, Canada, and their relationship to other dissolved constituents, oil and gas fields, and tectonic patterns. J. Geophys. Res. Solid Earth. 91, 12343–12353. https://doi.org/10.1029/JB091iB12p12343

Egger, M., Rasigraf, O., Sapart, C. J., Jilbert, T., Jetten, M. S. M., Röckmann, T., … Slomp, C. P., 2015. Iron-Mediated Anaerobic Oxidation of Methane in Brackish Coastal Sediments. Environ. Sci. Technol. 49, 277–283. https://doi.org/10.1021/es503663z

EPA, 2018. National Primary Drinking Water Regulations. Environmental Protection Agency, United States of America. https://www.epa.gov/ground-water-and-drinking-water/national-primary drinking-water-regulations#two. Accessed online November 11th, 2018.

Essaid, H.I., Bekins, B.A., Herkelrath, W.N., Delin, G.N., 2011. Crude Oil at the Bemidji Site: 25 Years of Monitoring, Modeling, and Understanding. Groundwater 49, 706–726. https://doi.org/10.1111/j.1745-6584.2009.00654.x

Fontenot, B.E., Hunt, L.R., Hildenbrand, Z.L., Carlton Jr., D.D., Oka, H., Walton, J.L., Hopkins, D., Osorio, A., Bjorndal, B., Hu, Q.H., Schug, K.A., 2013. An Evaluation of Water Quality in Private Drinking Water Wells Near Natural Gas Extraction Sites in the Barnett Shale Formation. Environ. Sci. Technol. 47, 10032–10040. https://doi.org/10.1021/es4011724

Forde, O.N., Mayer, K.U., Cahill, A.G., Mayer, B., Cherry, J.A., Parker, B.L., 2018. Vadose Zone Gas Migration and Surface Effluxes after a Controlled Natural Gas Release into an Unconfined Shallow Aquifer. Vadose Zone J. 17:180033. https://doi.org/10.2136/vzj2018.02.0033

Gorody, A.W., 2012. Factors affecting the variability of stray gas concentration and composition in groundwater. Environ. Geosci. 19, 17–31. https://doi.org/10.1306/eg.12081111013

Grossman, E.L., Cifuentes, L.A., Cozzarelli, I.M., 2002. Anaerobic Methane Oxidation in a Landfill-Leachate Plume. Environ. Sci. Technol. 36, 2436–2442. https://doi.org/10.1021/es015695y

Gülay, A., Musovic, S., Albrechtsen, H.J., Al-Soud, W.A., Sørensen, S.J., Smets, B.F., 2016. Ecological patterns, diversity and core taxa of microbial communities in groundwater-fed rapid gravity filters. ISME J. 9: 2209.

Gumm, L.P., Bense, V.F., Dennis, P.F., Hiscock, K.M., Cremer, N., Simon, S., 2016. Dissolved noble gases and stable isotopes as tracers of preferential fluid flow along faults in the Lower Rhine Embayment, Germany. Hydrogeol. J. 24:99-108. https:\\doi.org/10.1007/s10040-015-1321-7

Gurevich, A.E., Endres, B.L., Robertson, J.O., Chilingar, G.V., 1993. Gas migration from oil and gas fields and associated hazards. J. Pet. Sci. Eng. 9, 223–238. https://doi.org/10.1016/0920-4105(93)90016-8

Harrison, S.S., 1983. Evaluating System for Ground-Water Contamination Hazards Due to Gas-Well Drilling on the Glaciated Appalachian Plateau. Ground Water. 21, 689–700. https://doi.org/10.1111/j.1745-6584.1983.tb01940.x

Heron, G., Faulkner, B P., Mravik S.C., Wood, A.L., Gierke, J.S., Enfield., C.G., 2003. Pulsed Air Sparging in Aquifers Contaminated with Dense Nonaqueous Phase Liquids. Groundwater Monitor. Remed. 22, 73-82.

Hildenbrand, Z.L., Carlton, D.D., Fontenot, B.E., Meik, J.M., Walton, J.L., Taylor, J.T., Thacker, J.B., Korlie, S., Shelor, C.P., Henderson, D., Kadjo, A.F., Roelke, C.E., Hudak, P.F., Burton, T., Rifai, H.S., Schug, K.A., 2015. A Comprehensive Analysis of Groundwater Quality in The Barnett Shale Region. Environ. Sci. Technol. 49, 8254–8262. https://doi.org/10.1021/acs.est.5b01526

Humez, P., Mayer, B., Ing, J., Nighingale, M., Becker, V., Kingston, A., Akbilgic, O., Taylor, S., 2016a. Occurrence and Origin of Methane in Groundwater in Alberta (Canada): Gas Geochemical and Isotopic Approaches. Sci. Total Environ. 541, 1253–1268. http://dx.doi.org/10.1016/j.scitotenv.2015.09.055

Humez, P., Mayer, B., Nightingale, M., Becker, V., Kingston, A., Taylor, S., Bayegnak, G., Millot, R., Kloppmann, W., 2016b. Redox controls on methane formation, migration and fate in shallow aquifers. Hydrol. Earth Syst. Sci. 20, 2759–2777. https://doi.org/10.5194/hess-20-2759-2016

Kampbell, D.H., Wilson, J.T., Vandegrift, S.A., 1989. Dissolved Oxygen and Methane in Water by a GC Headspace Equilibration Technique. Int. J. Environ. Anal. Chem. 36, 249–257. https://doi.org/10.1080/03067318908026878

Kelly, W.R., Matisoff, G., Fisher, J.B., 1985. The effects of a gas well blow out on groundwater chemistry. Environ. Geol. Water Sci. 7, 205–213. https://doi.org/10.1007/BF02509921

Kenward, P.A., Simister, R.L., Morgan-Lang, C., Finke, N., Sturm, A., Hallam, S.J., Crowe, S.A., 2018. Recovering cellular biomass from fluids using chemical flocculation. Environ. Microbiol. Rep. 10, 686–694. https://doi.org/10.1111/1758-2229.12690

Kirtland, B. C., Aelion, C. M., 2000. Petroleum mass removal from low permeability sediment using air sparging/soil vapor extraction: impact of continuous or pulsed operation. J. Cont. Hydro. 41, 367–383. https://doi.org/10.1016/S0169-7722(99)00071-6

Kreuzer, R.L., Darrah, T.H., Grove, B.S., Moore, M.T., Warner, N.R., Eymold, W.K., Whyte, C.J., Mitra, G., Jackson, R.B., Vengosh, A., Poreda, R.J., 2018. Structural and Hydrogeological Controls on Hydrocarbon and Brine Migration into Drinking Water Aquifers in Southern New York. Groundwater. 56, 225–244. https://doi.org/10.1111/gwat.12638

Larson, T.E., Nicot, J.-P., Mickler, P., Castro, M.C., Darvari, R., Wen, T., Hall, C.M., 2018. Monitoring Stray Natural Gas in Groundwater With Dissolved Nitrogen. An Example From Parker County, Texas. Water Resour. Res. 54, 6024–6041. https://doi.org/10.1029/2018WR022612

Li, H., Carlson, K.H., 2014. Distribution and Origin of Groundwater Methane in the Wattenberg Oil and Gas Field of Northern Colorado. Environ. Sci. Technol. 48, 1484–1491. https://doi.org/10.1021/es404668b

MacFarlane, D.S., Cherry, J.A., Gillham, R.W., Sudicky, E.A., 1983. Migration of contaminants in groundwater at a landfill: A case study: 1. Groundwater flow and plume delineation. J. Hydrol., Migration of Contaminants in Groundwater at a Landfill: A Case Study 63, 1–29. https://doi.org/10.1016/0022-1694(83)90221-4

Mackay, D.M., Freyburg, D.L., Roberts, P.V., Cherry, J.A., 1986. A natural gradient experiment on solute transport in a sand aquifer 1. Approach and overvie of plume movement. Water Resour. Res., 22, 2017-2029.

Mayer, K. U., Benner, S. G., Frind, E. O., Thornton, S. F., Lerner, D. N., 2001. Reactive transport modeling of processes controlling the distribution and natural attenuation of phenolic compounds in a deep sandstone aquifer. J. Cont. Hydrol. 53, 341–368. https://doi.org/10.1016/S0169-7722(01)00173-5

McPhillips, L.E., Creamer, A.E., Rahm, B.G., Walter, M.T., 2014. Assessing dissolved methane patterns in central New York groundwater. J. Hydrol. Reg. Stud. 1, 57–73. https://doi.org/10.1016/j.ejrh.2014.06.002

Molofsky, L.J., Connor, J.A., McHugh, T.E., Richardson, S.D., Woroszylo, C., Alvarez, P.J., 2016. Environmental Factors Associated with Natural Methane Occurrence in the Appalachian Basin. Groundwater. 54, 656-668. https://doi.org/10.1111/gwat.12401

Ng, G.H.C., Bekins, B.A., Cozzarelli, I.M., Baedecker, M.J., Bennett, P.C., Amos, R.T., Herkelrath, W.N., 2015. Reactive transport modeling of geochemical controls on secondary water quality impacts at a crude oil spill site near Bemidji, MN. Water Resour. Res. 51, 4156–4183. https://doi.org/10.1002/2015WR016964

Nicholson, R.V., Cherry, J.A., Reardon, E.J., 1983. Migration of contaminants in groundwater at a landfill: A case study 6. Hydrogeochemistry. J. Hydrol. 63, 131–176. https://doi.org/10.1016/0022-1694(83)90226-3

Röling, W.F.M., van Verseveld, H.W., 2002. Natural attenuation: What does the subsurface have in store? Biodegradation. 13, 53–64. https://doi.org/10.1023/A:1016310519957

Roy, N., Molson, J., Lemieux, J.-M., Stempvoort, D.V., Nowamooz, A., 2016. Three-dimensional numerical simulations of methane gas migration from decommissioned hydrocarbon production wells into shallow aquifers. Water Resour. Res. 52, 5598–5618. https://doi.org/10.1002/2016WR018686

Sang, S., Zhang, X., Dai. H., Hu, B.X., Ou, H., Sun, L., 2018. Diversity and predictive metabolic pathways of the prokaryotic microbial community along a groundwater salinity gradient of the Pearl River Delta, China. Sci. Rep. 1: 17317.

Schout, G., Hartog, N., Hassanizadeh, S.M., Griffioen, J., 2017. Impact of an historic underground gas well blowout on the current methane chemistry in a shallow groundwater system. Proc. Natl. Acad. Sci. 115, 296-301. https://doi.org/10.1073/pnas.1711472115

Scow, K.M., Hicks, K.A., 2005. Natural attenuation and enhanced bioremediation of organic contaminants in groundwater. Curr. Opin. Biotechnol., Environmental biotechnology/Systems biology. 16, 246–253. https://doi.org/10.1016/j.copbio.2005.03.009 https://doi.org/10.1016/j.copbio.2005.03.009

Singer, V.L., Jones, L.J., Yue, S.T., Haugland, R.P., 1997. Characterization of PicoGreen reagent and development of a fluorescence-based solution assay for double-stranded DNA quantitation. Anal. Biochem. 249, 228-238.

Steelman, C.M., Klazinga, D.R., Cahill, A.G., Endres, A.L., Parker, B.L., 2017. Monitoring the evolution and migration of a methane gas plume in an unconfined sandy aquifer using time-lapse GPR and ERT. J. Contam. Hydrol. 205, 12–24. https://doi.org/10.1016/j.jconhyd.2017.08.011

Sudicky, E.A., 1986. A natural gradient experiment on solute transport in a sand aquifer: Spatial variability of hydraulic conductivity and its role in the dispersion process. Water Resour. Res. 22, 2069–2082. https://doi.org/10.1029/WR022i013p02069

Sudicky, E.A., Illman, W.A., 2011. Lessons learned from a suite of CFB Borden experiments. Ground Water. 49, 630–648. https://doi.org/10.1111/j.1745-6584.2011.00843.x

Unno, T., Kim, J., Kim, Y., Nguyen, S.G., Guevarra, R.B., Kim, G.P., Lee, J., Sadowsky. M.J., 2015. Influence of seawater intrusion on microbial communities in groundwater. Sci. Total Environ. 532, 337-343.

Van Stempvoort, D., Maathuis, H., Jaworski, E., Mayer, B., Rich, K., 2005. Oxidation of fugitive methane in ground water linked to bacterial sulfate reduction. Ground Water. 43, 187–199. https://doi.org/10.1111/j.1745-6584.2005.0005.x

Vengosh, A., Jackson, R.B., Warner, N., Darrah, T.H., Kondash, A., 2014. A Critical Review of the Risks to Water Resources from Unconventional Shale Gas Development and Hydraulic Fracturing in the United States. Environ. Sci. Technol. 48, 8334–8348. https://doi.org/10.1021/es405118y

Vidic, R.D., Brantley, S.L., Vandenbossche, J.M., Yoxtheimer, D., Abad, J.D., 2013. Impact of Shale Gas Development on Regional Water Quality. Science 340, 1235009. https://doi.org/10.1126/science.1235009

Voisin, J., Benoit C., Antonin V., Florian M.B., 2018. Aquifer recharge with stormwater runoff in urban areas: Influence of vadose zone thickness on nutrient and bacterial transfers from the surface of infiltration basins to groundwater. Sci. Total Environ. 637, 1496-1507.

Warner, N.R., Jackson, R.B., Darrah, T.H., Osborn, S.G., Down, A., Zhao, K., White, A., Vengosh, A., 2012. Geochemical evidence for possible natural migration of Marcellus Formation brine to shallow aquifers in Pennsylvania. Proc. Natl. Acad. Sci. U.S.A. 109, 11961–11966. https://doi.org/10.1073/pnas.1121181109

Whiticar, M.J., Faber, E., 1986. Methane oxidation in sediment and water column environments—Isotope evidence. Org. Geochem. 10, 759–768. https://doi.org/10.1016/S0146-6380(86)80013-4

Williams, G.M., Aitkenhead, N., 1991. Lessons from Loscoe: the uncontrolled migration of landfill gas. Q. J. Eng. Geol. Hydrogeol. 24, 191–207. https://doi.org/10.1144/GSL.QJEG.1991.024.02.03

Wolfe, A. L., Wilkin, R. T., 2017. Evidence of Sulfate-Dependent Anaerobic Methane Oxidation within an Area Impacted by Coalbed Methane-Related Gas Migration. Environ. Sci. Technol. 51, 1901–1909. https://doi.org/10.1021/acs.est.6b03709

Yan, B., Stute, M., Panettieri Jr., R.A., Ross, J., Mailloux, B., Neidell, M.J., Soares, L., Howarth, M., Liu, X., Saberi, P., Chillrud, S.N., 2017. Association of groundwater constituents with topography and distance to unconventional gas wells in NE Pennsylvania. Sci. Total Environ. 577, 195–201. https://doi.org/10.1016/j.scitotenv.2016.10.160

Zigah, P. K., Oswald, K., Brand, A., Dinkel, C., Wehrli, B., Schubert, C. J., 2015. Methane oxidation pathways and associated methanotrophic communities in the water column of a tropical lake. Limnol. Oceanogr. 60, 553–572. https://doi.org/10.1002/lno.10035

Figure Captions

Figure 1. A) Map of Canada with the location of Canadian Forces Base Borden in Ontario marked by a black dot. B) Monitoring network with multilevel wells (M1-M32) spanning 10 m down-gradient from the injection zone in the direction of groundwater flow. C) Cross-section along the injection line (A-A') of the Borden aquifer depicting hydrogeochemical conditions and landfill leachate with sampling points and injection screens at depth.

Figure 2. Log-log plot of average dissolved gas concentrations in groundwater from all multilevel wells sampled on respective days. Concentrations are given in mmol L^{-1} at 2 m (red), 6 m (blue), and 8 m (black) for $CH_{4(aq)}$, $CO_{2(aq)}$, and $N_{2(aq)}$ with time elapsed since injection. Baseline conditions are averaged from three sampling events (days -49, -21, and -2) and shown

as day 5. Maximum average concentrations for each depth and dissolved gas are marked with a black square. A dashed line from the baseline values is shown for each depth.

Figure 3. A) Stable carbon isotope ratios for CH_4 plotted versus $CH_{4(aq)}$ concentrations (mmol L^{-1}) from day 300, 500, and 700 at 2 m to 8 m depth. Elevated δ^{13}C-CH_4 values suggest the occurrence of $CH_{4(aq)}$ oxidation, particularly on day 500 at 8 m and 2 m bgs. Fractionation associated with diffusive migration is most evident from ^{12}C-enrichment at 2 m depth. B) Gas dryness (ratio of methane [C_1] to ethane [C_2] plus propane [C_3]) plotted versus δ^{13}C-CH_4 values from day 300, 500, and 700 for groundwater from 2 m to 8 m depth. Some samples where δ^{13}C-CH_4 > -20 ‰ did not have detectable C_2 and C_3 concentrations and are thus not included.

Figure 4. Log-log plot of average concentrations of redox indicator species in groundwater from all multilevel wells sampled on respective days. Concentrations are given in mmol L^{-1} at depths of 2 m (red), 6 m (blue), and 8 m (black). Baseline conditions are averaged from three sampling events (days -49, -21, and -2) and shown as day 5. A dashed line from the baseline value is shown for each depth.

Figure 5. Log-log plot of average concentrations of major ions in groundwater from all multilevel wells sampled on respective days. Concentrations are given in mmol L^{-1} at depths of 2 m (red), 6 m (blue), and 8 m (black). Baseline conditions are averaged from three sampling

events (days -49, -21, and -2) and shown as day 5. A dashed line from the baseline concentrations is shown for each depth.

Figure 6. A) Major ion composition for groundwater at baseline conditions and day 28. Groundwater composition changed on day 28 when EC increased above baseline. The composition at 2 m depth approached ratios similar to baseline conditions at 6 m depth. The composition at 6 m depth on day 28 was close to baseline groundwater from 8 m depth. B) Log-log plot of Cl versus SO_4^{2-} concentrations (mmol L^{-1}) in groundwater at 2 m (blue), 6 m (green), and 8 m (purple) depths from before, during, and post injection. Mixing lines based on Phreeqc simulations for samples from 2 m and 6 m depths and, 6 m and 8 m depths indicate mixing trends of groundwater from these depths during injection.

Figure 7. Log-log plot of average concentrations of trace elements in groundwater from all multilevel wells sampled on respective days. Concentrations are given in μmol L^{-1} at depths of 2 m (red), 6 m (blue), and 8 m (black). Baseline conditions are averaged from three sampling events (days -49, -21, and -2) and shown as day 5. A dashed line from the baseline concentrations is shown for each depth.

Figure 8. Conceptual model for the natural gas injection experiment. A) Active injection (day 0 to 72) led to an extensive free and dissolved phase CH_4 plume. Injection of free phase gas entrained groundwater from the landfill leachate plume at 9 m depth, leading to mixing with shallower water. B) Long-term (>300 days post injection) $CH_{4(aq)}$ persisted in the aquifer with an increase in microbially mediated $CH_{4(aq)}$ oxidation.

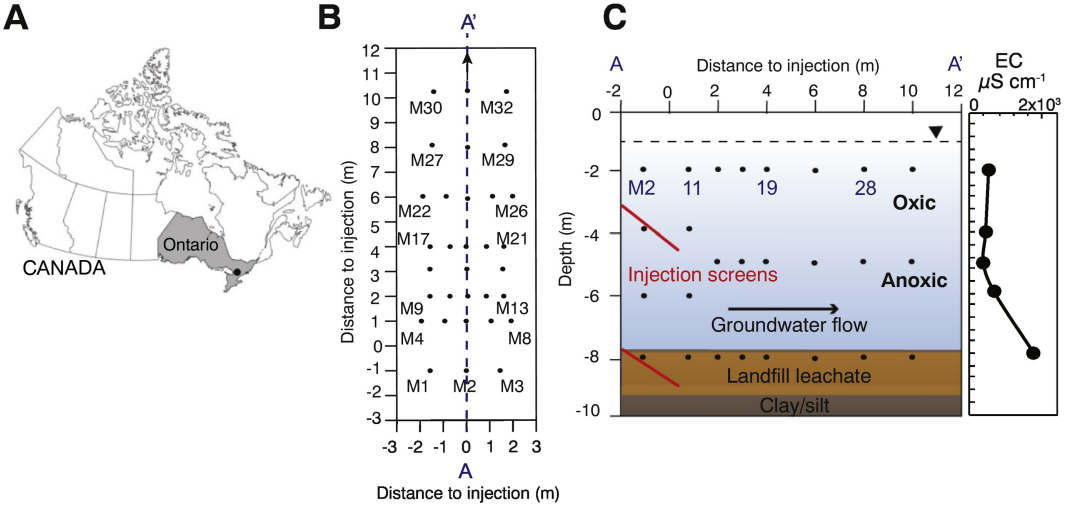
A
Ontario
CANADA
B
A'
M30
M32
M27
M29
M22
M26
M17
M21
M9
M13
M4
M8
M1
M2
M3
A
Distance to injection (m)
Distance to injection (m)
C
A
Distance to injection (m)
A'
EC
μS cm-1
2x10³
M2
11
19
28
Oxic
Anoxic
Injection screens
Groundwater flow
Landfill leachate
Clay/silt
Depth (m)

Figure 1

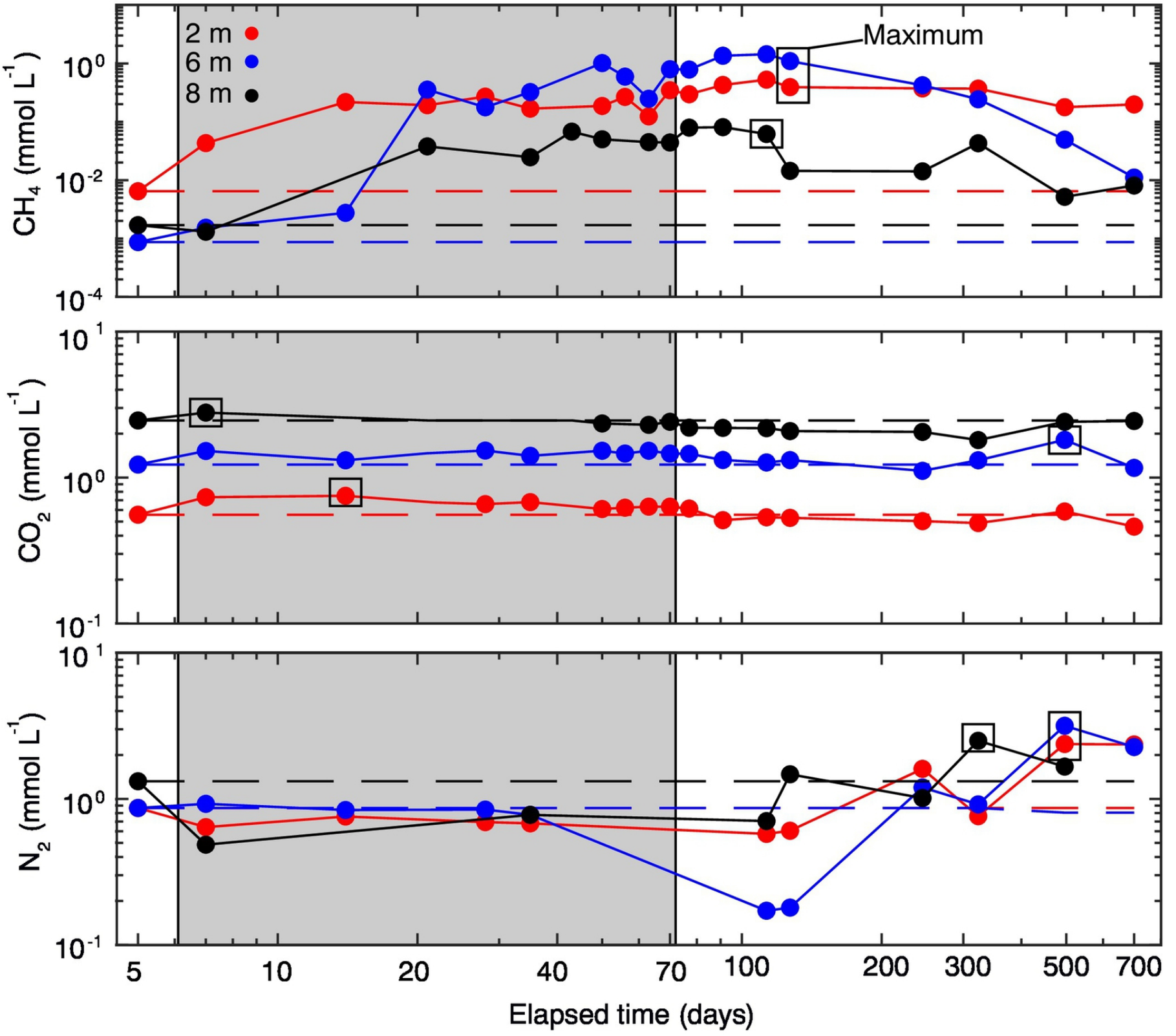
2 m
6 m
8 m
Maximum
CH_4 (mmol L^{-1})
CO_2 (mmol L^{-1})
N_2 (mmol L^{-1})
10^0
10^{-2}
10^{-4}
10^1
10^{-1}
5
10
20
40
70
100
200
300
500
700
Elapsed time (days)

Figure 2

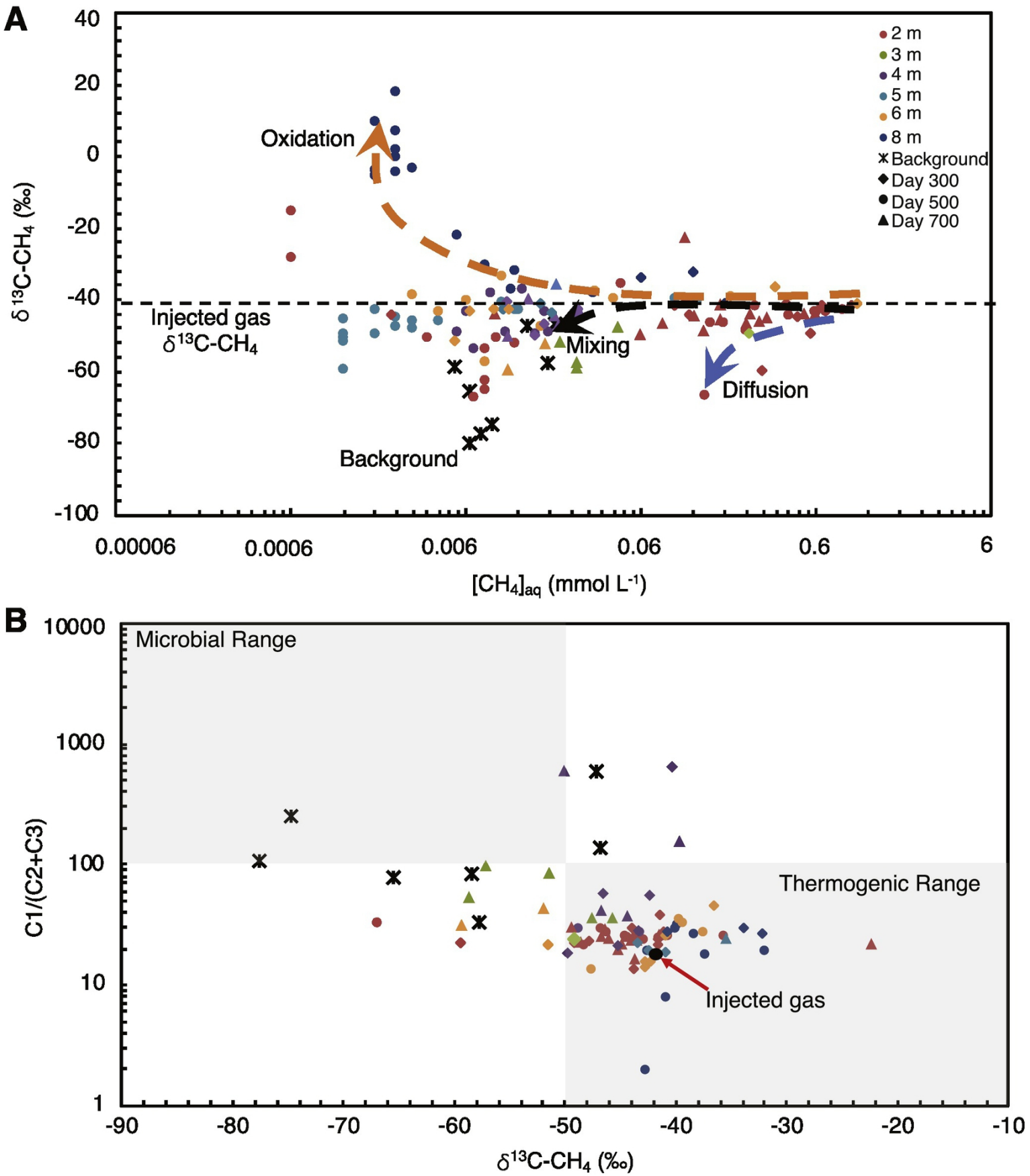
A
40
20
0
-20
-40
-60
-80
-100
δ13C-CH4 (‰)
2 m
3 m
4 m
5 m
6 m
8 m
Background
Day 300
Day 500
Day 700
Oxidation
Injected gas
δ13C-CH4
Mixing
Diffusion
Background
0.00006
0.0006
0.006
0.06
0.6
6
[CH4]aq (mmol L-1)
B
10000
1000
100
10
1
C1/(C2+C3)
Microbial Range
Thermogenic Range
Injected gas
-90
-80
-70
-60
-50
-40
-30
-20
-10
δ13C-CH4 (‰)

Figure 3

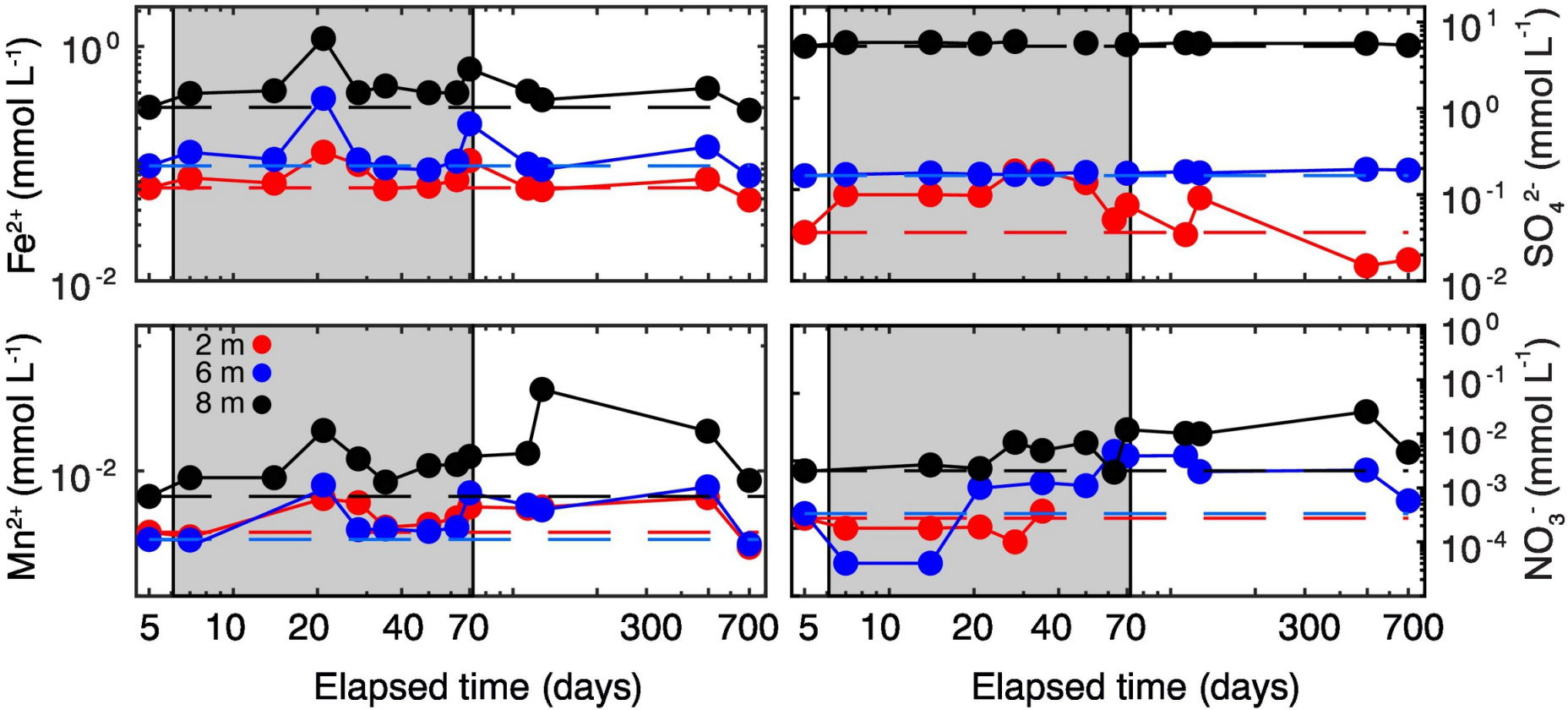
Fe2+ (mmol L-1)
Mn2+ (mmol L-1)
SO4 2- (mmol L-1)
NO3 - (mmol L-1)
2 m
6 m
8 m
5 10 20 40 70 300 700
Elapsed time (days)
5 10 20 40 70 300 700
Elapsed time (days)

Figure 4

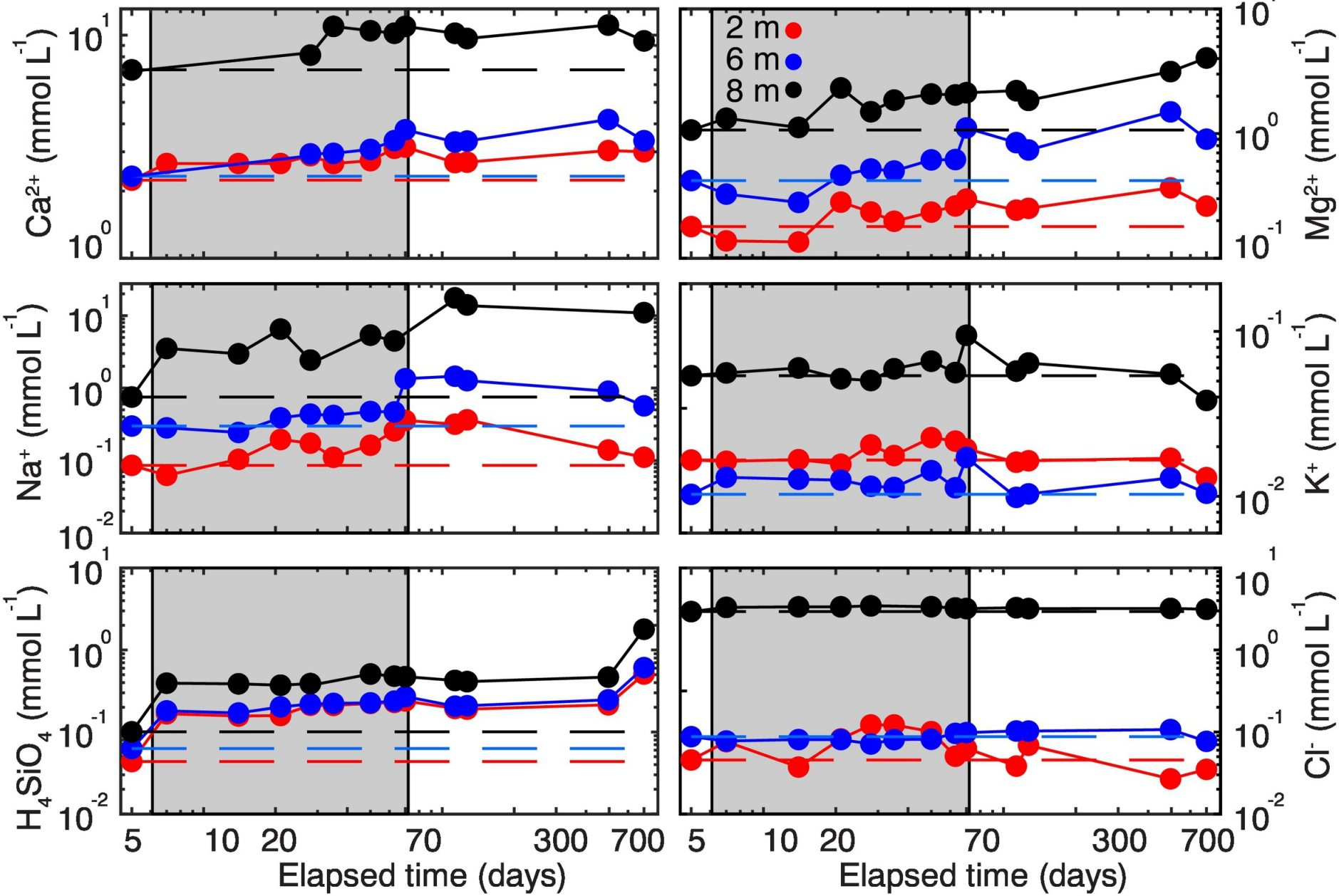
2 m
6 m
8 m
Ca2+ (mmol L-1)
Mg2+ (mmol L-1)
Na+ (mmol L-1)
K+ (mmol L-1)
H4SiO4 (mmol L-1)
Cl- (mmol L-1)
5
10
20
70
300
700
Elapsed time (days)
Elapsed time (days)

Figure 5

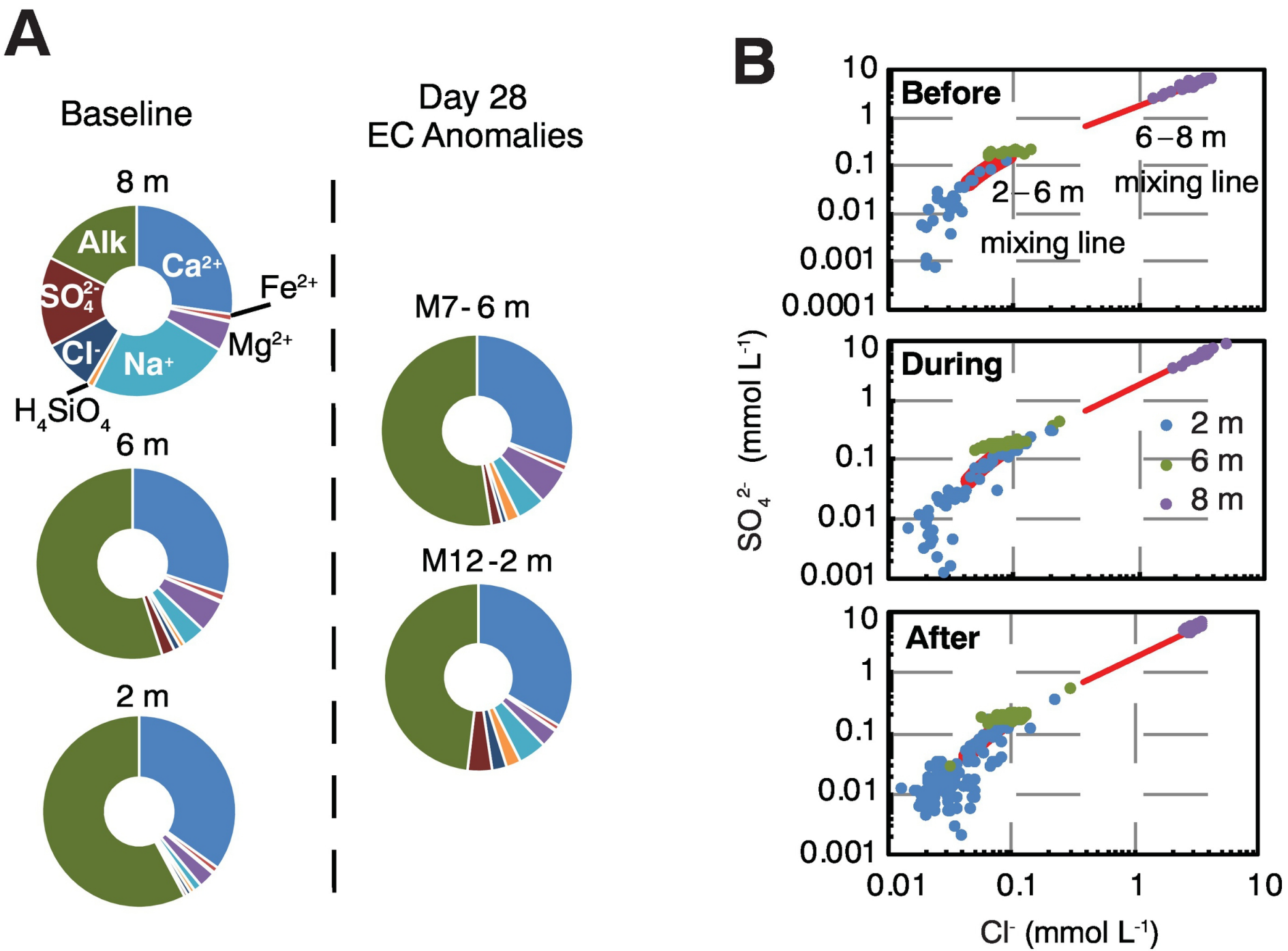
A
Baseline
Day 28
EC Anomalies
8 m
Alk
Ca2+
Fe2+
SO4 2-
Mg2+
Cl-
Na+
H4SiO4
6 m
2 m
M7 - 6 m
M12 - 2 m
B
Before
During
After
6 – 8 m
mixing line
2 – 6 m
mixing line
2 m
6 m
8 m
10
1
0.1
0.01
0.001
0.0001
0.01
0.1
1
10
SO4 2- (mmol L-1)
Cl- (mmol L-1)

Figure 6

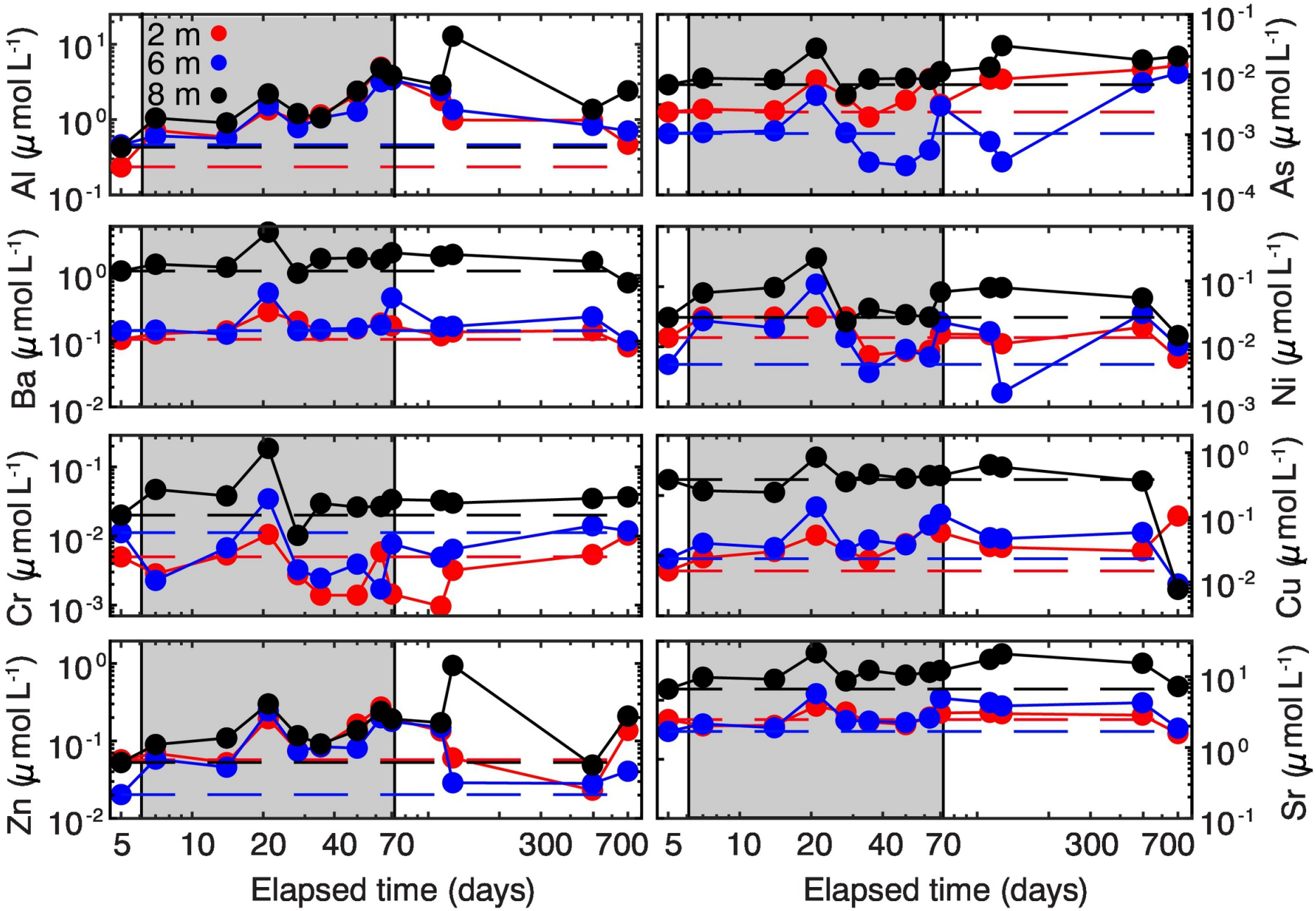
2 m
6 m
8 m
Al (μmol L-1)
As (μmol L-1)
Ba (μmol L-1)
Ni (μmol L-1)
Cr (μmol L-1)
Cu (μmol L-1)
Zn (μmol L-1)
Sr (μmol L-1)
5
10
20
40
70
300
700
Elapsed time (days)
Elapsed time (days)

Figure 7

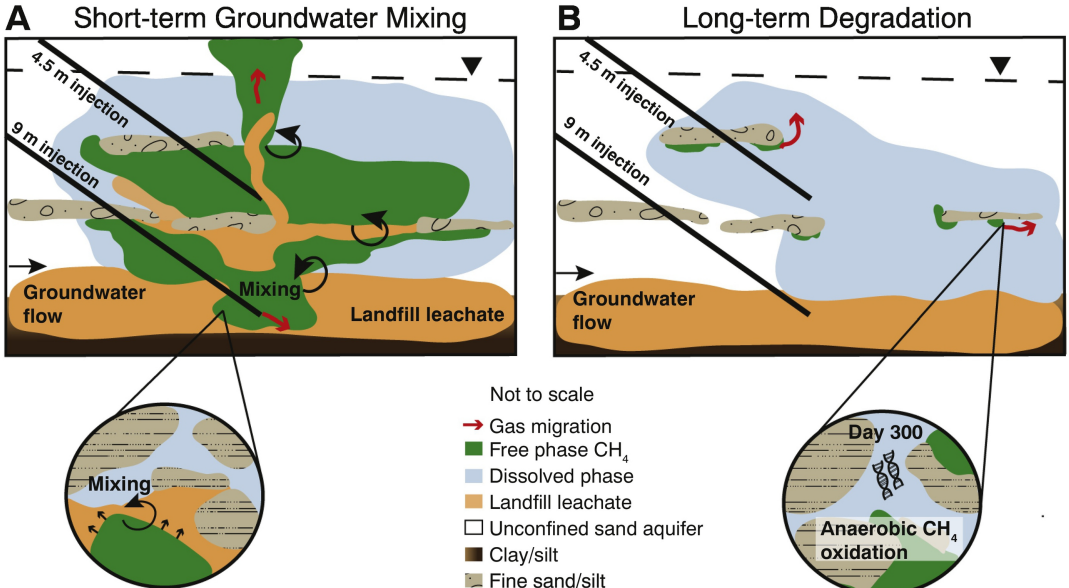
A
Short-term Groundwater Mixing
4.5 m injection
9 m injection
Groundwater flow
Mixing
Landfill leachate
B
Long-term Degradation
4.5 m injection
9 m injection
Groundwater flow
Mixing
Not to scale
Gas migration
Free phase CH4
Dissolved phase
Landfill leachate
Unconfined sand aquifer
Clay/silt
Fine sand/silt
Day 300
Anaerobic CH4 oxidation

Figure 8